

Discovery of a 5*H*-Benzo[4,5]cyclohepta[1,2-*b*]pyridin-5-one (MK-2461) Inhibitor of c-Met Kinase for the Treatment of Cancer

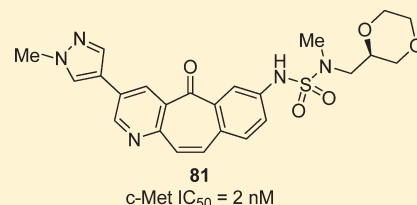
Jason D. Katz,^{*,†} James P. Jewell,[†] David J. Guerin,[†] Jongwon Lim,[†] Christopher J. Dinsmore,[†] Sujal V. Deshmukh,[#] Bo-Sheng Pan,[‡] C. Gary Marshall,[‡] Wei Lu,[‡] Michael D. Altman,^{||} William K. Dahlberg,[§] Lenora Davis,[‡] Danielle Falcone,[†] Ana E. Gabarda,[†] Gaozhen Hang,[‡] Harold Hatch,[‡] Rachael Holmes,[†] Kaiko Kunii,[⊥] Kevin J. Lumb,[○] Bart Lutterbach,[‡] Robert Mathvink,[†] Naim Nazef,[#] Sangita B. Patel,[○] Xianlu Qu,[⊥] John F. Reilly,[⊥] Keith W. Rickert,[○] Craig Rosenstein,[§] Stephen M. Soisson,[○] Kerrie B. Spencer,[†] Alexander A. Szewczak,[§] Deborah Walker,[▽] Wenxian Wang,[§] Jonathan Young,[†] and Qinwen Zeng[‡]

[†]Departments of Chemistry, [‡]Oncology, [§]In Vitro Pharmacology, ^{||}Structural Chemistry, [⊥]In Vivo Pharmacology, [#]Drug Metabolism and Pharmacokinetics, and [▽]Basic Pharmaceutical Sciences, Merck Research Laboratories, 33 Avenue Louis Pasteur, BMB-2-114, Boston, Massachusetts 02115, United States

[○]Global Structural Biology, Merck Research Laboratories, 770 Sumneytown Pike, West Point, Pennsylvania 19486, United States

S Supporting Information

ABSTRACT: c-Met is a transmembrane tyrosine kinase that mediates activation of several signaling pathways implicated in aggressive cancer phenotypes. In recent years, research into this area has highlighted c-Met as an attractive cancer drug target, triggering a number of approaches to disrupt aberrant c-Met signaling. Screening efforts identified a unique class of 5*H*-benzo[4,5]cyclohepta[1,2-*b*]pyridin-5-one kinase inhibitors, exemplified by **1**. Subsequent SAR studies led to the development of **81** (MK-2461), a potent inhibitor of c-Met that was efficacious in preclinical animal models of tumor suppression. In addition, biochemical studies and X-ray analysis have revealed that this unique class of kinase inhibitors binds preferentially to the activated (phosphorylated) form of the kinase. This report details the development of **81** and provides a description of its unique biochemical properties.



INTRODUCTION

c-Met, also referred to as hepatocyte growth factor receptor (HGFR), is a heterodimeric transmembrane receptor tyrosine kinase composed of an extracellular α chain and a membrane spanning β chain that are connected through a disulfide bond.^{1,2} The tyrosine kinase domain resides in the cytosolic portion of the β chain.^{1,2} Binding of the endogenous ligand, hepatocyte growth factor (HGF, also known as scatter factor), to c-Met induces dimerization of the c-Met receptors and triggers transphosphorylation (Y1234 and Y1235) and conformational changes that initiate the kinase activity.² The subsequent phosphorylation of a short peptide sequence near the C-terminus (Y1349, Y1356, and Y1365) forms a unique multisubstrate docking site that mediates activation of several signaling pathways, including PI3K-PDK1-AKT-mTor, Ras-Rac-Pak, Ras-Raf-MEK-ERK, and PLC- γ .²⁻⁴ In addition to the proliferative and antiapoptotic activities that are common to many other growth factors, HGF/c-Met signaling initiates unique motogenic and morphogenic phenotypes in c-Met expressing cells by stimulating cell–cell detachment, migration, invasiveness, and formation and branching of tubules.^{2,5,6}

c-Met was first identified as the oncogenic fusion Tpr-Met.⁷ A connection between c-Met and human cancer has been established in hereditary papillary renal carcinoma (HPRC), which is causally related to gain-of-function germline mutations in the c-Met

tyrosine kinase domain.^{8,9} Aberrant c-Met signaling, resulting from MET genomic amplification, c-Met or HGF overexpression, or c-Met mutations, is found in a variety of human cancers and often correlated with poor clinical outcomes.^{2,10} Recently, constitutive c-Met activation due to MET amplification was found to be a driver of proliferation and survival of several gastric and lung cancer cell lines^{11,12} and has been linked to acquired resistance of lung cancers to epidermal growth factor receptor (EGFR) inhibitors.^{13,14}

In recent years, research has highlighted c-Met as an attractive cancer drug target, triggering a number of approaches to disrupt HGF/c-Met signaling. Both small-molecule c-Met kinase inhibitors and antibodies targeting c-Met or HGF have exhibited antitumor activities in preclinical models.¹⁵⁻³⁰ The purpose of this report is to describe the discovery of a series of novel, ATP-competitive, small molecule inhibitors of c-Met that preferentially bind to the activated form of c-Met.³¹

Screening of the Merck compound collection identified *N*-(5-oxo-3-phenyl-5*H*-benzo[4,5]cyclohepta[1,2-*b*]pyridin-7-yl)methanesulfonamide (compound **1**, Figure 1) as a potent inhibitor of c-Met, with an IC₅₀ = 31 nM in our in vitro kinase assay.³¹ At the time that this work was initiated, we were not aware of any

Received: January 31, 2011

Published: May 24, 2011

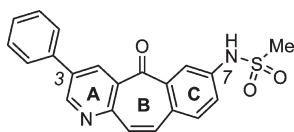
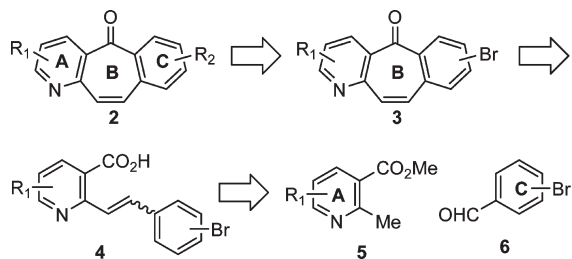


Figure 1. Structure of sulfonamide **1**.

reports indicating the use of 5H-benzo[4,5]cyclohepta[1,2-*b*]pyridin-5-one scaffolds as kinase inhibitors, which prompted the team to investigate this lead in more detail. Additional in vitro profiling indicated that **1** was an ATP competitive inhibitor of c-Met (e.g., at 0.05 mM ATP, IC_{50} = 31 nM; at 0.10 mM ATP, IC_{50} = 220 nM); however, initial molecular modeling experiments did not provide a satisfactory hypothesis of its binding mode in the ATP binding site. Further analysis indicated that while **1** displayed moderate activity in a cell-biochemical assay (GTL-16 pY1349 IC_{50} = 2,500 nM), it showed no modulation of cell proliferation, a key phenotype of the c-Met pathway. This was routinely measured in our screening funnel via measuring proliferation of GTL-16 cells over a 72 h period (**1**, IC_{50} > 50000 nM). Counterscreening against common off-target liabilities revealed that **1** was not an inhibitor of three major CYP isozymes (3A4, 2C9, 2D6 IC_{50} > 50 μ M), but there were some potential concerns with regard to Kv11.1 inhibition (Kv11.1 IC_{50} = 290 nM).³² Furthermore, **1** possessed suboptimal rat pharmacokinetic properties, with modest clearance (Cl_p = 24 mL/min/kg), short half-life ($t_{1/2}$ = 30 min), and minimal oral bioavailability (F = 2%).³³ In addition, the fused tricyclic core of **1** contributed to its poor physical properties ($\log P$ = 3.15; solubility at pH 7.4 = 0.5 μ g/mL). The purpose of this report is to detail our efforts to elucidate the structure–property relationships about the central 5H-benzo[4,5]cyclohepta[1,2-*b*]pyridin-5-one core of **1**. In addition, details are provided regarding the identification of compounds with increased potency and optimized pharmacokinetic properties that demonstrate their potential as chemotherapeutic agents.

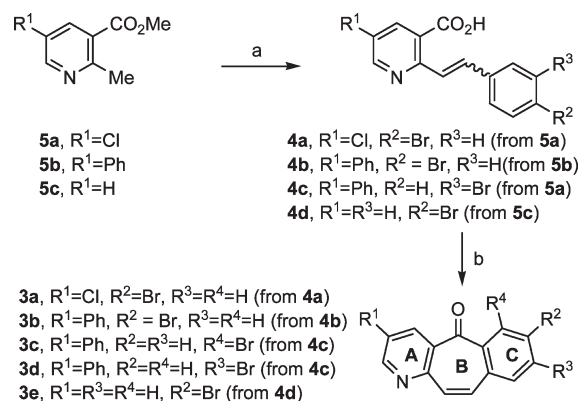
Scheme 1. Retrosynthetic Analysis of the 5H-Benzo[4,5]cyclohepta[1,2-*b*]pyridin-5-one Core 2



CHEMISTRY

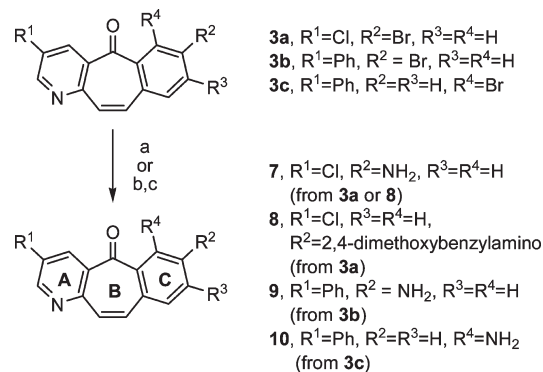
A general retrosynthetic analysis for the construction of the 5H-benzo[4,5]cyclohepta[1,2-*b*]pyridin-5-one core is presented in Scheme 1. In this approach, the final substituted 5H-benzo[4,5]cyclohepta[1,2-*b*]pyridin-5-ones **2** were prepared via palladium catalyzed C–C and/or C–N bond forming events from the bromo intermediates **3**. The seven-membered core B of **3** was available via the intramolecular Friedel–Crafts cyclization of the 2-vinylphenyl nicotinic acids **4**. This key cyclization substrate was

Scheme 2. Synthesis of the 5H-Benzo[4,5]cyclohepta[1,2-*b*]pyridin-5-one Core Compounds 3a–e^a



^a (a) **6**, KO^{*t*}-Bu, THF, 0 °C; (b) polyphosphoric acid, 200 °C.

Scheme 3. Incorporation of Amines into C Ring of 3^a

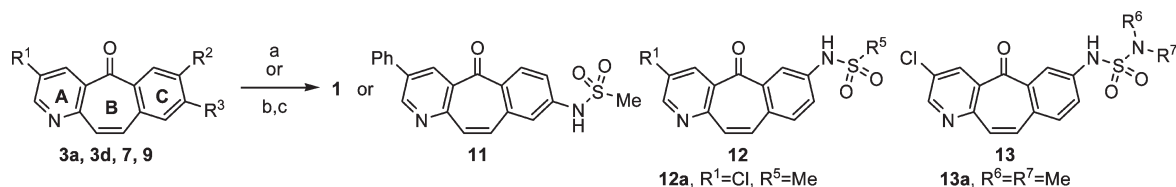


^a (a) Benzophenone imine, Pd₂(dba)₃, NaOt-Bu, toluene, 110 °C, 2.5 h; then THF, 6N HCl; (b) 2,4-dimethoxybenzylamine, Pd₂(dba)₃, NaOt-Bu, 1,4-dioxane, 100 °C, 2.5 h; (c) TFA, DCM.

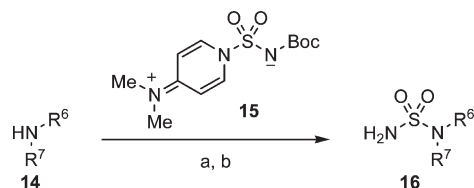
formed via the condensation/dehydration of the substituted 2-methyl nicotinic acids **5** with the appropriate bromobenzaldehydes **6**. The following descriptions of the synthetic routes (Schemes 2–7) provide a concise overview of the methods employed to access the target compounds.³⁴

As shown in Scheme 2, the core synthesis began with the base induced condensation/dehydration of the substituted 2-methyl nicotinic acids **5a–c**,³⁵ with the appropriate bromobenzaldehyde **6** to give the cyclization substrates **4a–d**. Subsequent heating of the functionalized 3-carboxyl-pyridines **4a–d** in polyphosphoric acid (PPA) at 200 °C facilitated the intramolecular Friedel–Crafts cyclization to form the core seven-membered ring B in **3a–e**.³⁶ In the case of the unsymmetrical bromide **4c**, the cyclization results in the formation of the regioisomers **3c** and **3d** in approximately a 1:1 ratio.

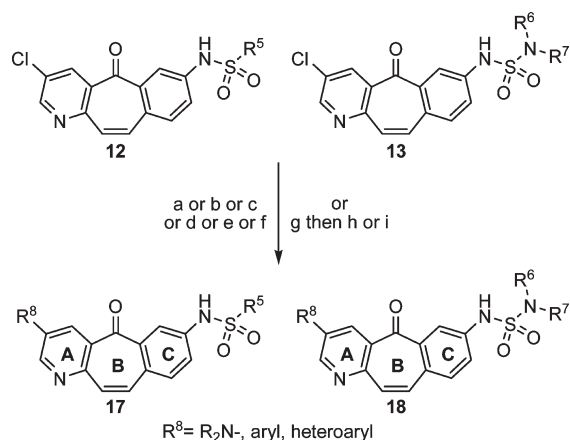
Upon formation of the tricyclic core, it was possible to derivatize the bromide on the C ring. As shown in Scheme 3, the arylbromide **3** could be converted to the primary aniline via palladium-mediated coupling with benzophenone imine, followed by immediate acid-mediated hydrolysis of the intermediate imine to give **7** and **10**.³⁷ The bromide could also be converted in a similar manner to a variety of amines, exemplified by the conversion to the dimethoxybenzylamine derivative **8**,

Scheme 4. Incorporation of Sulfonamides and Sulfamides into the C Ring^a

^a (a) 3a or 3d, sulfonamide or sulfamide, Pd₂(dba)₃, Xantphos, Cs₂CO₃, 1,4-dioxane, 100 °C; (b) 7 or 9, alkyl- or aryl-sulfonylchloride, NEt₃, DCM; (c) THF, 5N NaOH.

Scheme 5. Synthesis of Substituted Sulfamides^a

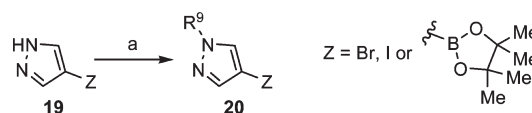
^a (a) 15, NEt₃, DCM; (b) TFA, DCM.

Scheme 6. Functionalization of the A Ring^a

^a (a) R⁸-1° or 2° amine, Pd₂(dba)₃, NaOt-Bu, 1,4-dioxane, 100 °C; (b) R⁸-1° or 2° amine, Pd₂(dba)₃, Cs₂CO₃, DMF, 180 °C μw; (c) R⁸-boronic acid or ester, Pd(PPh₃)₄, K₂CO₃, 1,4-dioxane, 100 °C; (d) R⁸-boronic acid or ester, PdCl₂(dppf), K₂CO₃, dioxane, 95 °C; (e) R⁸-boronic acid or ester, Pd₂(dba)₃, P(*t*-Bu)₃·HBF₄, KF, DMF, 100 °C; (f) R⁸-boronic acid or ester, Pd₂(dba)₃, P(*t*-Bu)₃·HBF₄, KF, DMF, 180 °C μw; (g) (pinB)₂, Pd₂(dba)₃, (C₆H₁₁)₃P, KOAc, 1,4-dioxane, 100 °C; (h) R⁸-halide, Pd(PPh₃)₄, K₂CO₃, DMF, 185 °C, μw; (i) R⁸-halide Pd₂(dba)₃, P(*t*-Bu)₃·HBF₄, KF, DMF, 100 °C.

which could also be converted to the aniline 7 via treatment with TFA (also 3b→9).

Similarly, the C ring bromide 3 could be converted into a wide array of substituted sulfonamides and sulfamides via palladium-mediated cross-coupling chemistry (Scheme 4). Initially, the sulfonamides were installed by a stepwise approach, involving bis-sulfonylation of the anilines (e.g., 7→12a), followed by treatment with NaOH to affect partial hydrolysis of one sulfonyl group to deliver the monoarylsulfonamides 12. At the outset of the program, this approach allowed exploration of a wide array of functionality on the C ring beyond the sulfonamide moiety found in 1. However, anilines such as 7 proved to be poor nucleophiles

Scheme 7. Synthesis of *N*-Alkyl or *N*-Arylpyrazoles^a

^a (a) R⁹-X, base, CH₃CN or DMF; X = Cl, I, OMs, or OTf.

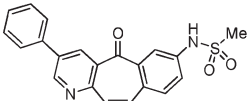
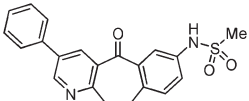
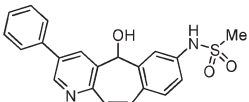
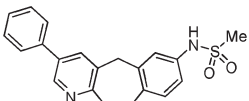
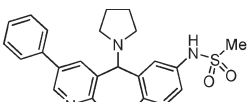
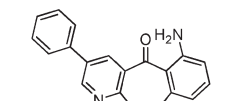
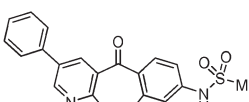
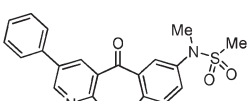
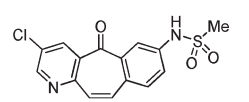
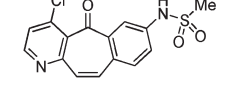
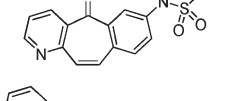
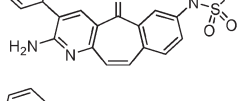
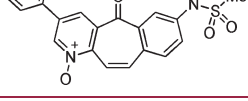
and did not couple effectively to elaborated sulfonyl or sulfamoyl chlorides, which hindered an in-depth exploration about the sulfonyl moiety (vide infra). Instead, a method was adopted that involved direct conversion of the aryl bromide to the corresponding arylsulfonamide (11, 12) or arylsulfamide (13) via a palladium-mediated coupling with the corresponding primary sulfonamide or sulfamide.³⁸ The requisite sulfamides required for the coupling were prepared from the corresponding secondary amines using the method described by Montero (14→16, Scheme 5).³⁹

With the derivatization of the C ring complete, it was now possible to functionalize the pyridyl ring (A ring). To that end, the chloride in 12 or 13 could be converted to a substituted aniline by utilizing various palladium-mediated amination strategies (Scheme 6, conditions a or b).^{40–42} While both sets of conditions delivered the desired aniline, condition a often resulted in either significant proto-dehalogenation or reduction of the carbonyl in the B ring. In contrast, for certain amine coupling partners, condition b minimized these side reactions and would be used instead. Similarly, the A ring pyridylchloride could be converted to an aryl or heteroaryl derivative via palladium-mediated cross-coupling with the corresponding boronic acid or ester. While a number of conditions were explored for this transformation (Scheme 6, conditions c, d, e, or f), those described by Fu proved to be the most general and usually resulted in the highest conversion to desired product.⁴³ In a few cases (R⁸ = *N*-substituted pyrazole), the required R⁸ boronic esters or acids were not commercially available and one of two synthetic strategies were adopted. In the first case, the chloride 13 was converted to the boronic acid and subsequently coupled to the corresponding halopyrazole. In the second strategy, the *N*-substituted-pyrazole boronic esters or halides 20 were accessed via the *N*-alkylation/arylation of the parent pyrazole 19 with a suitable R⁹ group (Scheme 7).

RESULTS AND DISCUSSION

Key Modifications of the Tricyclic Core of 1. Because the 5*H*-benzo[4,5]cyclohepta[1,2-*b*]pyridin-5-one core of 1 had not been described previously in the kinase literature, one of the initial priorities was to explore the scaffold and its potential

Table 1. SAR about the Central 5*H*-Benzo[4,5]cyclohepta-[1,2-*b*]pyridin-5-one Core of 1

	Structure	c-Met IC ₅₀ (nM)
1		31
21		2,300
22		>10,000
23		2,800
24		770
10		1,100
11		>10,000
25		780
12a		380
26		>10,000
27		1,100
28		6,100
29		3,000

binding mode via targeted modifications around the periphery of the 6,7,6-tricyclic core. The effects of some of these fundamental structural changes to **1** on the ability to inhibit the function of

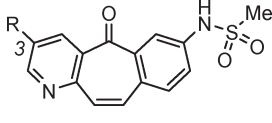
c-Met are summarized in Table 1.⁴⁴ Changes to the central seven-membered ring resulted in a significant decrease in potency against c-Met. Saturation of the double bond, as in **21**, resulted in a 70-fold drop in potency. Similarly, reduction of the carbonyl to either the alcohol **22** or the methylene derivative **23** resulted in a significant loss of activity. Further derivatization of **22** to tertiary amines such as **24** delivered compounds more potent than the parent alcohol but significantly less active than **1**. At the outset of this effort, the origins of this very narrow SAR were not well-understood. However, molecular modeling results indicated that the core of **1** had a high degree of planarity and all of these modifications likely resulted in a central B ring that was significantly puckered (vide infra). Given that **1** was an ATP competitive inhibitor and likely bound to the hinge region of the ATP binding site, it is reasonable to assume that significant changes to the planarity of the core could impact ligand binding affinity to c-Met.

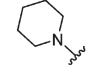
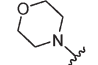
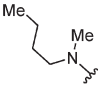
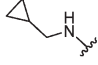
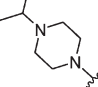
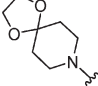
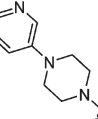
The position of the aniline on the C ring was also important for retaining c-Met activity. Moving the pharmacophore from the 7-position to the 6- or 8-position, as with compounds **10** and **11**, resulted in c-Met IC₅₀ values of 1100 nM and >10000 nM, respectively (for a discussion of the aniline as a pharmacophore in this scaffold, refer to Table 4). Simple alkylation of sulfonamide **1** (*N*-methyl sulfonamide **25**) led to a 25-fold loss in potency, indicating that the sulfonamide N–H may be involved in key hydrogen bonding interactions, although other possibilities could be inferred (e.g., conformational bias, steric interaction in the binding site, etc.). Along with other data not shown, these results indicated that the original position of the sulfonamide pharmacophore was optimal for c-Met activity.

Selected modifications of the A ring of **1** revealed a similarly narrow SAR. Replacement or deletion of the phenyl ring, such as in the aryl chloride **12a** or the proto-derivative **27**, resulted in a loss of activity on the same order of magnitude observed for other core alterations. However, the relatively moderate 12-fold loss in potency for the chloride **12a** indicated that this position might be a promising site for additional modifications. In contrast, moving the substitution to other positions on the pyridyl ring completely eroded the activity such as with the 4-chloropyridine derivative **26**. Finally, simple changes to the pyridine indicated that the *N*-1 atom was important for binding to c-Met, as conversion to the 2-amino-pyridine derivative **28** or the *N*-oxide **29** led to a 200- and 100-fold loss in activity, respectively. The erosion of potency with the *N*-oxide **29** would be expected if the pyridine was involved in making key hinge interactions in the ATP binding pocket. However, the results with **28** were more surprising, as amino-pyridines making two hydrogen bonds to the hinge are common in the kinase literature. Eventually, a crystal structure allowed for a more complete analysis of this particular facet of the SAR (vide infra). Overall, the modifications detailed in Table 1 emphasized that the integrity of the tricyclic-heptenone core of **1** needed to be maintained; however, they also revealed that the phenyl and sulfonamide positions could be targeted for further exploration.

Initial Substitutions at the 3-Position of the A Ring. An initial goal of the early SAR about **1** was to identify compounds that were more potent both in the primary HTRF c-Met assay as well as the GTL-16 cell-biochemical assay. The GTL-16 cell line is a gastric cancer cell line which harbors MET genomic amplification and overexpresses constitutively activated c-Met protein.⁴⁵ For reasons that will be discussed below, inhibition in this cell line was measured by monitoring levels of the C-terminal

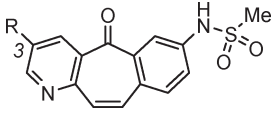
Table 2. SAR of Amino Derivatives at the 3-Position

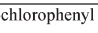
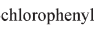
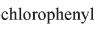
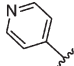
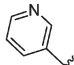
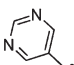
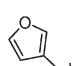
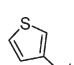
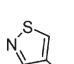
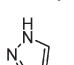
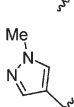


R	c-MetIC ₅₀ (nM)	GTL-16 pY1349 IC ₅₀ (nM)
	93	1,100
	46	2,000
	440	8,000
	89	760
	32	140
	24	790
	16	2,000

docking site pY1349.³¹ The above modifications to the core of **1** (Table 1) indicated that a reasonable initial strategy would be to explore derivatives at the 3-position of the pyridine ring. Given that the poor physical properties (e.g., solubility, log *P*, protein binding) of **1** potentially contributed to its poor cellular activity, amine analogues at the 3-pyridyl position were targeted to address these issues (Table 2). Initial results appeared promising, as the piperidinyl derivative **30** (ACD log *P* = 1.8) was 2.5-fold more active in the cellular assay even though it displayed 3-fold less intrinsic potency compared to that of **1** (ACD log *P* = 2.0). In general, cyclic tertiary amines, such as **30** and the morpholino analogue **31** displayed similar intrinsic *c*-Met activity compared to **1** and exhibited a more favorable cell-shift. In contrast, tertiary acyclic amines such as the *N*-butyl-*N*-methyl derivative **32** proved to be less active, although this was not general, as the cyclopropylmethyl derivative **33** retained some of this potency. One of the first compounds with promising activity in the cellular assay was the isopropylpiperazine analogue **34** (ACD log *P* = 1.5), which retained the intrinsic activity of **1** but was nearly 20-fold more active in the cellular assay. Related amines, such as the bicyclic ketal **35** or the 2-piperazinylpyridine **36**, showed notably increased cell shifts. While amino compounds such as **34** satisfied the initial goal of identifying potent compounds in the GTL-16 cell-biochemical assay, further characterization revealed that most of the amino analogues displayed poor rat pharmacokinetics (typically Cl_p > Q_{hep}). Ultimately, this subseries was deprioritized in favor of new modifications described below.

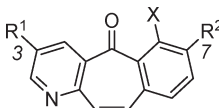
Table 3. SAR of Aryl and Heteroaryl Derivatives at the 3-Position

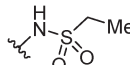
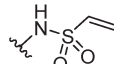
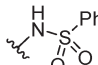
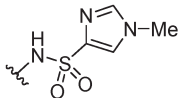
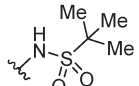
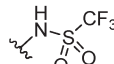
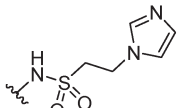
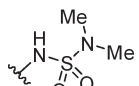


R	c-Met IC ₅₀ (nM)	GTL-16 pY1349 IC ₅₀ (nM)
	280	9,000
	45	5,300
	46	5,400
	30	750
	74	2,500
	180	9,000
	64	5,500
	10	1,500
	14	210
	170	1,400
	4	12

Aryl and heteroaryl derivatives at the 3-position of **1** were being investigated in parallel with the amino analogues. As a general trend, 2-substituted arenes were much less potent than the 3- and 4-substituted analogues (e.g., 2-, 3-, and 4-chloro analogues **37**, **38**, and **39**, respectively), potentially by forcing the phenyl group farther out of plane with the cycloheptenone core (Table 3). Incorporation of six-membered heteroaryl groups, such as the 4-pyridyl group in **40**, improved both the solubility and cell-shift, but related compounds such as the 3-pyridyl **41** and the pyrimidinyl **42** were not as well tolerated. On the other hand, incorporation of five-membered heterocyclic analogues led to a much more promising series of compounds. A significant increase in both intrinsic *c*-Met activity and GTL-16 cell-shift was observed in going from the 3-furanyl **43** to the 3-thienyl **44** and finally the thiazolyl **45**. Further screening of heterocycles, such as the *N*-H pyrazole **46**, revealed that this effect was not general; however, we were pleased to observe that the *N*-methylpyrazolyl **47** displayed superior activity compared to any of the previous compounds in the program and displayed only a 3-fold shift in the cell-biochemical assay. In addition, **47** displayed improved activity compared to historical compounds in the GTL-16 72 h

Table 4. SAR at the Methanesulfonamide Position



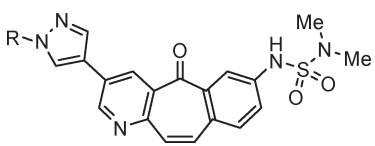
	R ¹	R ²	X	c-Met IC ₅₀ (nM)	GTL-16 pY1349 IC ₅₀ (nM)
48	<i>N</i> -methylpyrazole	-NH ₂	H	0.7	110
49	<i>N</i> -methylpyrazole	-NH ₂	Cl	19	360
50	<i>N</i> -methylpyrazole	-NHMe	H	5	80
51	<i>N</i> -methylpyrazole	-OH	H	11	370
52	Phenyl		H	27	1,500
53	Phenyl		H	130	9,000
54	Phenyl		H	390	9,000
55	<i>N</i> -methylpyrazole		H	100	2,300
56 ^a	<i>N</i> -methylpyrazole		H	31	580
57	<i>N</i> -methylpyrazole		H	2,600	5,500
58	<i>N</i> -methylpyrazole		H	13	7,300
59	<i>N</i> -methylpyrazole		H	4	80

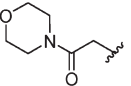
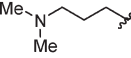


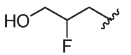
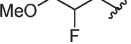
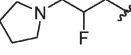
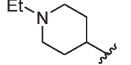
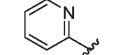
^a Final compound was judged to be 85% pure; see Supporting Information for full details.

proliferation assay (IC₅₀ = 1900 nM for **47** vs IC₅₀ > 50000 nM for **1**). These encouraging results raised the possibility that **47** could be further evaluated in various in vivo models of c-Met activity (e.g., tumor xenografts). Even though **47** exhibited suboptimal rat pharmacokinetics (Cl_p = 40 mL/min/kg, t_{1/2} = 30 min), it was the poor physical properties of the molecule (solubility leading to formulation issues) that prevented the execution of these experiments. Thus, while the *N*-methyl pyrazole group greatly improved the overall activity of this class of compounds, there were still many issues with the series yet to be resolved. In addition to physical properties, some of the detrimental off-target issues exhibited in **1**, such as Kv11.1 activity, were still present in **47** (Kv11.1 IC₅₀ = 10100 nM; I_{Kr} patchclamp IC₅₀ = 330 nM³²). Regardless, the methylation of the

pyrazole was a key result (**47** vs **46**) that warranted further investigation. Efforts to solve some of the issues with the scaffold via various *N*-substituted pyrazoles are presented later in this report.

Initial SAR of the 7-Position. The initial SAR about the core of **1** (Table 1) had indicated that the original 7-position of the sulfonamide in **1** was preferred. As such, the team had begun to explore analogues of the sulfonamide at the 7-position concurrently with the above efforts on the 3-position. Initial results revealed that the methane sulfonamide was not required for c-Met activity. In fact, with an IC₅₀ = 0.7 nM, the aniline **48** was approximately 7-fold more potent than the parent sulfonamide **47** (Table 4). However, this change eroded the cell-shift of the parent and **48** performed disappointingly in both rat and dog pharmacokinetic studies, with Cl_p ≫ Q_{hep}. Close

Table 5. SAR of *N*-substituted Pyrazoles


	R	c-Met IC ₅₀ (nM)	GTL-16 pY1349 IC ₅₀ (nM)	GTL-16 72h proliferation
60	<i>n</i> -propyl	2	ND	780
61		2	290	1,700
62		4	96	1,100
63		3	27	370
64		3	40	610
65		1	85	270
66		3	20	54
67		2	12	ND
68		0.2	74	55
69		130	750	1,300

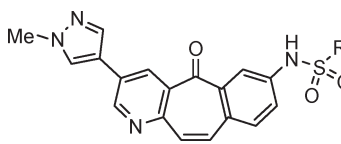
analogues of the aniline, such as the 2-chloro analogue **49**, *N*-Me aniline **50**, and the phenol **51**, were prepared for comparison. Unfortunately, these compounds were significantly less potent and exhibited a pharmacokinetic profile similar to the aniline. Subsequent efforts uncovered a number of suitable replacements for the sulfonamide and these other endeavors will be reported in future communications. However, the rest of this report will detail activities to develop the sulfonamide pharmacophore.

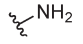
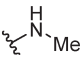
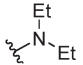
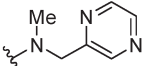
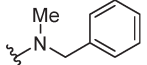
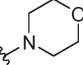
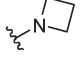
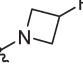
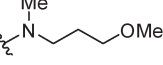
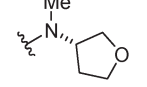
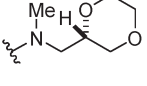
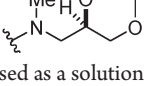
Initial exploration of the methane sulfonamide itself was not at all promising. While simple variations such as the ethylsulfonamide **52** were tolerated, other seemingly similar analogues such as the vinyl sulfonamide **53** resulted in a loss of activity against c-Met (Table 4). Indeed, it became apparent that sulfonamides with a sp² hybridized carbon adjacent to the sulfonyl were not preferred, such as with the phenyl sulfonamide **54** or the imidazolyl sulfonamide **55**. On the other hand, sp³ hybridized carbons adjacent to the sulfonyl were more consistently tolerated, as even the bulky *tert*-butyl sulfonamide **56** only suffered a 7-fold loss in potency vs **47**. The pK_a of the sulfonamide *N*-H also seemed to be integral to the ability of the scaffold to bind to the kinase, as the trifluoromethyl sulfonamide **57** was inactive

relative to the parent methane sulfonamide **47**.⁴⁷ Subsequent sp³ hybridized carbon analogues revealed that there was room in the binding site to extend out from the sulfonyl and still retain potency against c-Met, such as with the 2-imidazolyl-ethyl sulfonamide **58**, but they lacked adequate potency in cellular assays. On the other hand, incorporation of a nitrogen atom adjacent to the sulfonyl, as with the sulfamide **59**, resulted in a compound that was equipotent to the methane sulfonamide **47**. Further characterization of **59** revealed that it had a nearly identical compound profile to **47** (PK characteristics, cellular activity, physical properties, etc.) with one key exception. Sulfamide **59** did not have any of the Kv11.1 liabilities associated with the methane sulfonamide (Kv11.1 IC₅₀ > 30000 nM; I_{Kr} patchclamp IC₅₀ > 30000 nM).⁴⁶ Because *in vitro* activity against this ion channel had been a persistent problem with this series, the sulfamide functionality offered an opportunity to both explore new space in the binding region and attenuate off-target liabilities and physical properties. This prospect was explored by preparing two distinct sets of analogues of **59**: (1) a series where the sulfamide group was held constant and the pyrazole functionality was varied, and (2) a series where the *N*-methyl pyrazole was fixed and the sulfamide group was diversified.

Effect of *N*-substitution of the Pyrazole. Previous efforts had identified *N*-methyl pyrazole as a more potent compound than the corresponding *N*-H analogue (**47** vs **46**). To explore this in more detail, an array of *N*-substituted pyrazoles were prepared to see if further elaboration could attenuate the functional activity and the pharmacokinetic properties of the parent sulfamide **59**. Simple alkyl substitution, such as the *n*-propyl analogue **60** (Table 5), resulted in a slight boost in c-Met activity that also translated into enhanced functional activity (GTL-16 proliferation). A range of functional groups were well tolerated at this position, including pendant amides (**61**), amines (**62**), and alcohols (**63**), potentially due to this region extending out of the ATP binding pocket into a solvent exposed region. In particular, the alcohol **63** was interesting because it was one of the first compounds with an IC₅₀ < 500 nM in the GTL-16 proliferation assay; however, the pharmacokinetic properties of all of these analogues were still suboptimal. Metabolite ID of both **47** and **59** indicated that *N*-demethylation of the pyrazole was one route for biotransformation of the parent.⁴⁸ Consequently, several strategies were investigated to address this issue, such as preparing fluoroalkyl derivatives (**64–67**), constraining part of the alkyl system into a ring (**68**), and direct attachment of a heteroaryl substituent (**69**). Several of these analogues turned out to be some of the most potent compounds prepared at the time. However, these pyrazole analogues still suffered from poor pharmacokinetic profiles and efforts were directed toward other strategies.

Structural Variation of the Sulfamide. While substitution of the pyrazole did not identify a compound with a balanced profile (potency, physical properties, pharmacokinetics), exploration of the sulfamide of **59** proved to be more productive. Initial SAR focused on small variations of the sulfamide framework (Table 6). While both the –NH₂ analogue **70** and the monomethyl variant **71** retained the activity of the parent, other monosubstituted sulfamides were less potent (data not shown). Conversely, *N,N*-disubstitution of the sulfamide was well-tolerated and a range of activities was observed. Both the diethyl analogue **72** and the pyrazinylethyl **73** retained good activity, in contrast to both the benzyl **74** and the morpholinyl **75** analogues, which lost significant potency against c-Met. Gratifyingly, most of the sulfamide analogues retained their favorable Kv11.1 profile, although these derivatives still displayed relatively poor rat pharmacokinetic

Table 6. SAR of the *N*-Substituents of the Sulfamide


R	c-Met IC ₅₀ (nM)	GTL-16 pY1349 IC ₅₀ (nM)	GTL-16 72h proliferation	Kv11.1 IC ₅₀ (μM)	Rat PK Parameters			
					Cl _p (mL/min/kg)	V _{d,ss} (L/kg)	t _{1/2} (h)	F (%)
	3	12	990	4.3	ND	ND	ND	ND
	2	12	750	>30	33.8 ^a	2.5	0.9	33
	4	110	2,200	>30	ND	ND	ND	ND
	2	75	1,100	7.1	39 ^b	2.4	0.7	ND
	30	1,200	>50,000	>30	ND	ND	ND	ND
	58	1,000	11,000	ND	ND	ND	ND	ND
	10	71	1,100	>30	6.1 ^c	0.95	3.3	29
	5	28	2,400	>30	2.9 ^d	0.41	1.8	ND
	3	58	1,500	>30	10.7 ^e	1.1	1.3	ND
	2	53	570	>30	11.0 ^f	1.1	1.2	38
	14	210	2,800	>30	ND	ND	ND	ND
	2	56	440	>30	9.1 ^g	0.4	0.8	62

^a *n* = 3; dosed as a solution in DMSO:PEG400:water:ethanol (20:25:40:15); iv at 2 mg/kg; po at 4 mg/kg. ^b *n* = 1; dosed as a solution in PEG400:40% Captisol (35:65) with 1.2 equiv methanesulfonic acid; iv at 2 mg/kg. ^c *n* = 2; dosed as a solution in propylene glycol:40% Captisol:water (25:55:20) with 1.2 equiv KOH; iv and po at 1 mg/kg. ^d *n* = 2; dosed as a solution in propylene glycol:PEG400:40% Captisol (15:40:45) with 1.2 equiv methanesulfonic acid; iv at 2 mg/kg. ^e *n* = 2; dosed as a solution in propylene glycol:PEG400:40% Captisol (15:35:50); iv at 2 mg/kg. ^f *n* = 3; dosed as a solution in DMSO:PEG400:40% Captisol:water (10:20:50:20) with 2.2 equiv methanesulfonic acid; iv at 0.31 mg/kg and po at 0.62 mg/kg. ^g *n* = 4; dosed as a solution in 0.5% methylcellulose; iv at 2 mg/kg and po at 5 mg/kg.

properties. Further in vitro metabolite ID studies indicated that monoalkylation of the sulfamide was a major route of biotransformation,⁴⁹ and it was believed that certain cyclic analogues might reduce this metabolic pathway. Satisfyingly, the azetidine analogues **76** and **77** displayed an improved rat pharmacokinetic profile relative to **59**, with low plasma clearance, acceptable V_d, and an improved half-life. In addition, certain acyclic alkyl ethers (**78**) exhibited a similarly enhanced PK profile

relative to **59**. Unfortunately, these analogues were still limited by micromolar IC₅₀ values in cell-based functional assays. Eventually, it was found that cyclic ethers offered a balance between acceptable cell-based activities and pharmacokinetic properties. Screening a series of cyclic ethers led to the identification of the (*R*)-dioxanyl analogue **81** (MK-2461³¹), a potent inhibitor of the c-Met. Compared to the initial tricyclic lead, **81** displayed superior cell potency (GTL-16 IC₅₀ = 56 nM, GTL-16 72 h proliferation =

440 nM) and excellent rat pharmacokinetic properties ($Cl_p = 10$ mL/min/kg, $t_{1/2} = 1.3$ h). In general, **81** had a balanced PK profile across species (Table 7), with moderate Cl_p and suitable bioavailability, consistent with acceptable human PK predictions. While high Cl_p was observed in the mouse, this did not hinder profiling in animal models (vide infra). In addition to favorable PK properties, **81** offered a suitable balance of off-target activities and physical properties. It was free of Kv11.1 liabilities (Kv11.1 $IC_{50} > 30000$ nM; I_{Kr} patchclamp $IC_{50} > 30,000$ nM), as well as minimal potential for drug–drug interactions (CYP3A4, 2C9, 2D6 $IC_{50} = 7.1, 1.2, >100$ μ M, respectively). While optimizing from **1** to **81**, the log P was lowered from 3.15 to 2.70 and the ligand binding efficiency (LBE) only marginally decreased from 0.38 to 0.34. Finally, while the solubility of the free base was only slightly improved to 3 μ g/mL, various salt forms displayed solubility in excess of 100 mg/mL. Because of this balanced profile, as well as the properties described below, **81** was ultimately selected as the first clinical candidate for this program.

Unique Binding Mode of the Benzo[4,5]cyclohepta[1,2-*b*]pyridin-5-one Scaffold. At the same time that the tricyclic class was evolving toward a potent inhibitor of c-Met with suitable drug-like properties, a series of in vitro biochemical experiments identified some unique properties of this class of compounds, as reported in a recent communication.³¹ While **81** was competitive with ATP and thus likely bound in the ATP binding pocket, it displayed a unique signature of inhibition for various phosphotyrosine residues on the kinase. In particular, in a cell-free biochemical assay (cytosolic domain), **81** was more effective at inhibiting phosphorylation of the C-terminal docking site residues Y1349 ($IC_{50} \approx 100$ nM) and Y1365 ($IC_{50} \approx 26$ nM) than the autophosphorylation of the activation loop residues Y1230/1234/1235 ($IC_{50} \approx 900$ nM). This unique

signature was maintained in the GTL-16 cell line. Treatment of these cells potently inhibited phosphorylation of Y1349 and Y1365 in the c-Met C-terminal domain ($IC_{50} \approx 50$ nM) and inhibited phosphorylation of both AKT and ERK1/2, downstream signaling molecules of c-Met pathway.³¹ In contrast, treatment of these cells with **81** had almost no inhibitory effect on phosphorylation of the c-Met activation loop residues Y1234 and Y1235 ($IC_{50} > 2500$ nM).³¹ The fact that **81** was inefficient at inhibiting phosphorylation of the activation loop but was a potent inhibitor of phosphorylation at other regions on the protein suggested that it was preferentially binding to a form of the kinase with an activated (phosphorylated) activation loop. A second set of experiments designed to directly measure the binding of **81** to both the phosphorylated and unphosphorylated forms of the protein helped to confirm this hypothesis. Specifically, a series of BIAcore experiments revealed that these compounds preferentially bind to the activated form of the kinase ($K_d = 4$ nM) versus the unphosphorylated form ($K_d = 25$ nM).³¹ This data, combined with a series of molecular modeling and cocrystal structures, allowed a complete picture of the binding of these molecules and their mode of action to emerge.

Crystal Structure of Tricyclic Inhibitor **82 Bound to the Phosphorylated c-Met Kinase Domain.** Recently, the crystal structure of a structurally related tricyclic analogue of **81** bound to the doubly autophosphorylated domain of c-Met, in which Y1234 and Y1235 are phosphorylated, was reported.⁵⁰ This closely related tricyclic analogue, identified as **83** in this report (Figure 2), displays many of the binding properties ascribed to **81**, such as preferential binding to the autophosphorylated form of the kinase. However, it contained a very different pharmacophore at the 7-position of the core (ethylene linked amide).⁵⁰ In contrast, the tricyclic sulfamide analogue **82** differs from **81** only in the pyrazole *N*-alkyl substituent at the 3-position of the core (Figure 2).

The X-ray crystal structure of **82** bound to the dually phosphorylated kinase domain of c-Met was determined to 2.3 Å resolution (see Supporting Information Table S1). Upon binding **82**, the kinase domain adopts a very similar overall conformation to that observed upon binding **83**.⁵⁰ In both ligand-bound structures, Y1234 and Y1235 are phosphorylated, the activation loop is ejected from the ATP binding site, and the G loop adopts an extended induced-fit conformation that packs against the ligand to form part of the binding site (Figure 3A). The closely related analogues, **82** and **83**, bind in the ATP binding pocket in very similar orientations.

The structure of **82** bound to the autophosphorylated c-Met kinase domain confirms many of the previous hypotheses of the binding mode of this class of compounds (vide supra). In particular, the pyridine nitrogen of the core forms a hydrogen bond with the hinge backbone NH of M1160. In this orientation, the pyrazole extends along the hinge and its piperidine substituent projects out into solvent. Other key hydrogen bonds are made

Table 7. Pharmacokinetic Profile of **81**

	mouse (<i>n</i> = 2)	rat (<i>n</i> = 4)	dog (<i>n</i> = 4)	monkey (<i>n</i> = 2)
iv Parameters				
dose (mg/kg)	1 ^a	2 ^b	1 ^b	0.25 ^a
AUC _(0–∞) (μ M·h)	0.4	7.6	8.4	1.0
Cl_p (mL/min/kg)	83	9.1	4.3	8.4
V _{dss} (L/kg)	3.2	0.4	1.1	0.5
$t_{1/2}^1$ (h)	0.5	0.8	2.9	0.8
po Parameters				
dose (mg/kg)	2 ^a	5 ^c	2 ^c	0.5 ^a
AUC _(0–∞) (μ M·h)	0.6	11.8	13.7	0.4
C_{max} (μ M)	0.41	4.2	2.5	0.12
t_{max} (h)	0.3	0.7	1.4	3
bioavailability (%)	75	62	85	19

^a Dosed as a solution in 0.9% saline. ^b Dosed as a solution in 0.5% methylcellulose. ^c Dosed in PEG400:captisol:water (25:50:25 (v/v/v)).

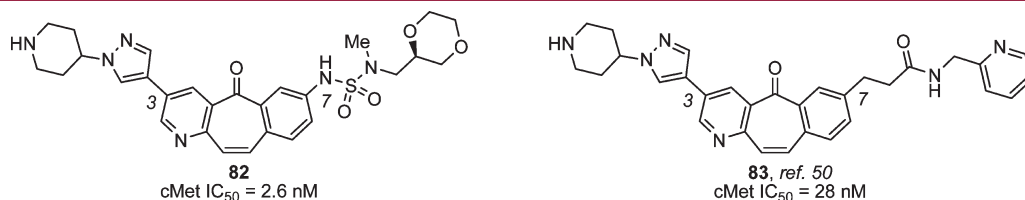


Figure 2. Ligands **82** and **83**.

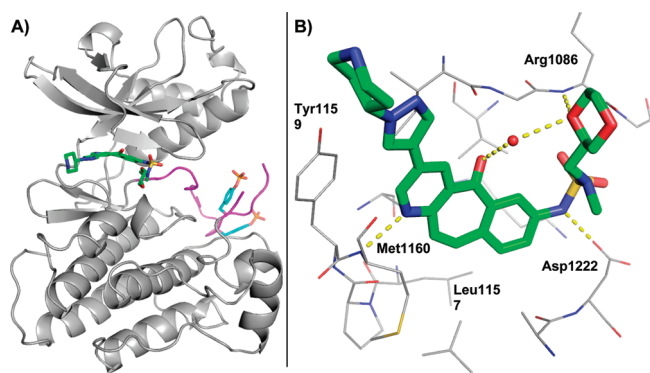


Figure 3. (A) Ribbon cartoon image of the X-ray crystal structure of **82** (green) bound to activated c-Met kinase domain (gray). The activation loop (magenta) and pY1234 and pY1235 (cyan) are also highlighted. (B) Binding pose of **82** in the ATP binding pocket.

between: (1) the aromatic NH of the sulfamide and the side chain of D1222 and (2) one of the dioxanyl oxygens and the backbone NH of R1086. As with the previously reported structure of the complex with **83**, the central carbonyl of the core is involved in a water-mediated hydrogen bond to the more proximal dioxanyl oxygen. Finally, the aromatic tricyclic core adopts a conformation that is only 22° out of planarity, as measured by the angle between the planes of the pyridyl and phenyl rings about the central troponone ring.

The binding mode for **82** agrees well with the observed general SAR for the benzo[4,5]cyclohepta[1,2-*b*]pyridin-5-one chemical series described in this report. For example, the slightly bent geometry for the tricyclic core may be critical in allowing potent analogues to bind in the ATP binding site (e.g., **1** and **81**). In contrast, compounds **21**–**24** are predicted by ab initio calculations⁵¹ to be locked into a more severely bent geometry, likely due to reduction of the aromatic character of the central 7-membered ring, thus precluding them from binding as effectively in the ATP pocket. Additionally, the poor potency of compounds **10**, **11**, and **25** can be explained by disruption of the interaction between the sulfamide NH and the catalytic aspartate side chain. Compounds **12a**, **26**, and **27** likely have reduced activity due to the lack of hydrophobic packing interactions in the hinge region that is provided by the phenyl or methylpyrazole groups. Finally, compounds **28** and **29** are expected to disrupt the hydrogen bond between the pyridine nitrogen and the backbone of the hinge region. While it is obvious that the *N*-oxide in **29** would disrupt this bonding, it is less clear when considering **28**. In **82**, the carbon at the 2-position is 2.9 Å from the carbonyl oxygen of M1160, consistent with a potential C–H hydrogen bonding interaction with the backbone carbonyl. As such, substitution at the 2-position, such as with the $-\text{NH}_2$ of **28**, may result in a clash with the hinge. The observed binding orientation also agrees well with many of the more subtle modifications made throughout the lead optimization process, including: (1) the preference for aryl groups at the 3-position (Tables 2 and 3) to maximize hydrophobic packing and planarity, (2) the tight SAR observed upon introduction of the sulfonamide/sulfamide group (Table 4) likely due to the burial of this region near the catalytic residues and the glycine rich loop (in compound **57**, the sulfonamide nitrogen is likely deprotonated, leading to its substantially poorer activity due to a loss of hydrogen bonding⁴⁷),

Table 8. c-Met Mutant Profile of 81

enzyme	IC ₅₀ (nM)
WT c-Met	2
N1100Y	1.5
Y1230C	1.5
Y1230H	1.0
Y1235D	0.5
M1250T	0.4

Table 9. Kinase Selectivity Profile of 81

kinase ^a	IC ₅₀ (nM) ^b	kinase ^a	IC ₅₀ (nM) ^b
Met	2	FGFR3	50
Ron	7	TrkB	61
Flt1	10	FGFR1	65
Flt3	22	Flt4	78
Mer	24	JAK2	230
FGFR2	39	Aur-A	290
KDR	44	Ret	640
TrkA	46	Abl	7,800

^a Human enzyme. ^b Average of $n = 2$.

and (3) the relatively flat SAR observed in Table 5, as these substituents are expected to be solvent exposed.

Activity against Mutant Forms of c-Met. There have been several reports in the literature of oncogenic mutations of c-Met that confer resistance to small molecule inhibitors of c-Met.^{15,16,31,52,53} Because this tricyclic series of compounds displayed a profound effect on c-Met signaling via residues outside of the activation loop, while having little effect on activation loop phosphorylation, the *in vitro* properties of **81** were compared against some of these mutations. As can be seen in Table 8, **81** maintained potency against a spectrum of these mutations, including several activation loop mutations. While there have been no reports discussing these mutations with respect to treatment in a clinical setting, it stands to reason that a compound that was insensitive to acquired mutations in the kinase might be an advantage in the treatment of c-Met dependent tumors.^{52,54}

Kinase Selectivity Profile of 81. With any kinase inhibitor, understanding the off-target kinase inhibition is crucial, especially to help interpret both efficacy and potential side effects. In general, the sulfonamide and sulfamide compounds in this report display a similar kinase selectivity profile. As can be seen in Table 9, **81** displays <100 nM activity against several other kinases, including some that might prove beneficial in a clinical setting, such as Ron, KDR, FGFR, and PDGFR- α . Even though **81** was found to be selective for the phosphorylated form of c-Met, this was shown to not be the case in several of the other kinases in this panel.³¹ In particular, **81** was shown to inhibit phosphorylation of the activation loop of both FGFR2 and PDGFR, indicating that it is capable of binding to the unactivated forms of these kinases. As such, while **81** is primarily an inhibitor of c-Met, it is also a multikinase inhibitor. In particular, inhibition of FGFR2 and PDGFR- α has potential implications for further development of this series of compounds. When tested against a panel of tumor cell lines, compound **81** was especially efficacious at inhibiting cell lines that had either genomic amplification of c-Met or FGFR2 or constitutive activation of PDGFR.³¹

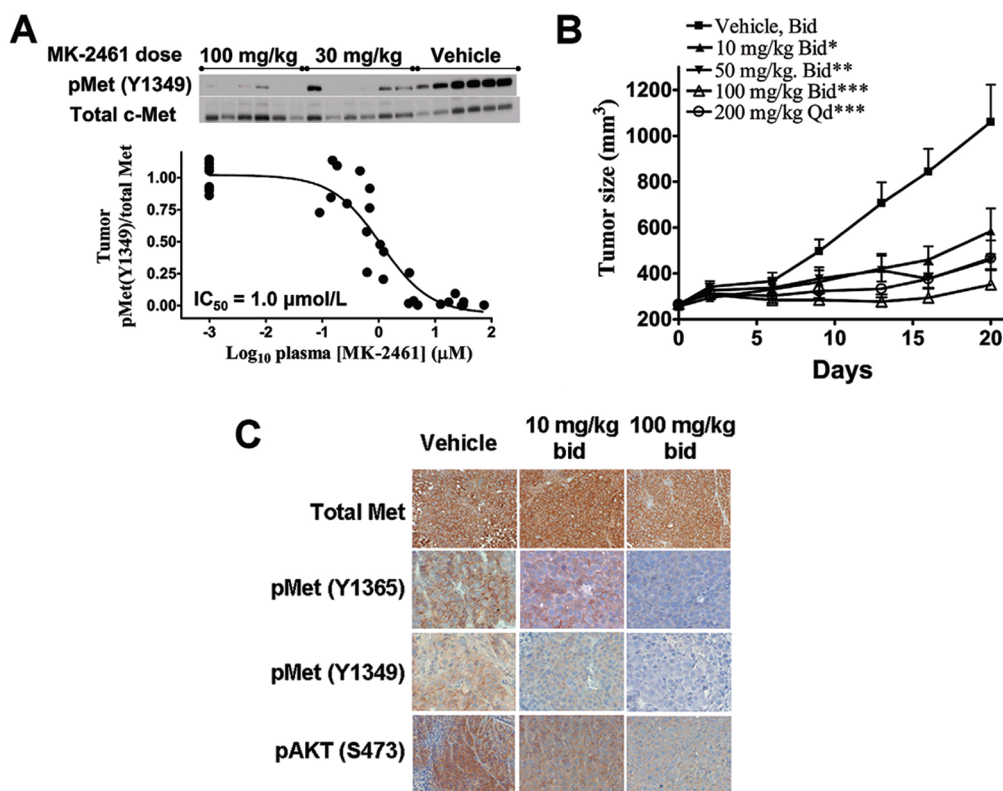


Figure 4. Compound **81** inhibited c-Met and AKT and suppressed the growth of xenograft tumors in nude mice. (A) Inhibition by **81** of c-Met (Y1349) phosphorylation in GTL-16 tumors. The tumor bearing mice were given a single oral dose of 3, 10, 30, or 100 mg/kg of **81** and euthanized 1 h after dosing. The extent of c-Met (Y1349) phosphorylation in the tumors was determined by quantitative Western blotting. Shown are representative images of phospho-c-Met (Y1349) and total c-Met blots. Also shown is the relationship between the phospho-c-Met (Y1349) levels of all individual tumors and the corresponding host plasma total **81** concentrations. (B) The effects of orally administered **81** on the growth of GTL-16 tumor. Asterisks indicate statistically significant difference from vehicle-treated group based on two-way repeated measures ANOVA (* $P \leq 0.05$, ** $P \leq 0.01$, *** $P \leq 0.001$). (C) Immunostaining for phospho-c-Met (Y1349), phospho-c-Met (Y1365), and phospho-AKT (S473) in GTL-16 xenograft tumors following 21-day dosing with vehicle or **81**. Tissues were collected at 4 h after the last dose.

In Vivo Studies of 81. As discussed above, identifying compounds in this series with an acceptable balance of potency, physical properties, and pharmacokinetics was a challenge that often hindered evaluation of the compounds in xenograft models. However, several sulfamides with pendant ethers (e.g., **78**, **79**, **81**) displayed an improved pharmacokinetic profile that warranted further evaluation of in vivo efficacy.

Cell-biochemical and cell-proliferation assays were conducted in a GTL-16 cell line, a cell line dependent on c-Met for survival. While the inhibition of GTL-16 cell proliferation and other ex vivo readouts can indicate c-Met pathway inhibition, it was necessary to establish c-Met dependent efficacy in vivo. In addition, it was not known if the novel mode of action of this new class of kinase inhibitors would translate to an in vivo model. A correlation between in vitro/in vivo target engagement, pathway inhibition, and efficacy was necessary to develop a strategy to eventually move these compounds into the clinical setting. It should be noted that while **81** had a relatively high plasma clearance and short half-life in the mouse (see Table 7), it was still possible to achieve exposures suitable for assessing efficacy in our mouse xenograft models.

As such, an acute PK/PD study of GTL-16 tumor-bearing CD1 nu/nu mice was performed, with the animals receiving **81** orally at four doses (3, 10, 30, and 100 mg/kg). Inhibition of c-Met was observed in vivo, with a plasma IC₅₀ = 1.0 μM, assessed at 1 h postdose (Figure 4A). This confirmation of target

engagement (inhibition of pY1349) in vivo led to the evaluation of **81** in a longer-term tumor xenograft efficacy study. In this experiment, the compound was dosed orally (10, 50, and 100 mg/kg bid; 200 mg/kg qd) in a 21 day GTL-16 xenograft study in CD1 nu/nu mice. As can be seen in Figure 4B, all doses from this study resulted in statistically significant suppression of tumor growth. The compound was well tolerated, and no change in median body weight was observed (data not shown). As in the acute PK/PD experiment, evidence of a dose-dependent inhibition of c-Met in the tumor was observed in this experiment. IHC analysis of the tumor samples at 4 h postdose (Figure 4C) showed inhibition of both c-Met and a downstream marker of pathway inhibition, AKT. This indicates that even though **81** inhibits c-Met via a unique mode of action, it still displays an inhibitory effect on the downstream pathway.

CONCLUSION

The *5H*-benzo[4,5]cyclohepta[1,2-*b*]pyridin-5-ones have been shown to be potent inhibitors of c-Met both in vitro and in vivo. This series of compounds exemplify a unique type of kinase inhibitors that preferentially bind to the phosphorylated form of c-Met. Investigations into this series of compounds have elucidated the structural basis of this selective inhibition and identified the requirements for kinase inhibition. Incorporation of

both the *N*-methyl pyrazole and the dioxanyl sulfamide functionality were crucial to achieving a balance between cell-based activity and an acceptable pharmacokinetic profile. In addition, the sulfamide functionality alleviated Kv11.1 activity inherent to this structural class. Sulfamide **81** has a balanced pharmacokinetic profile and has been shown to be efficacious in mouse tumor xenograft experiments. Future communications will detail additional evaluation of this new series of kinase inhibitors.

EXPERIMENTAL SECTION

Chemistry. Commercial reagents were obtained from commercial suppliers and used as received. All solvents were purchased in septum-sealed bottles stored under an inert atmosphere. All reactions were sealed with septa through which an argon atmosphere was introduced unless otherwise noted. Liquid reagents and solvents were transferred under a positive pressure of argon via syringe. Reactions were conducted in microwave vials or round-bottomed flasks containing Teflon-coated magnetic stir bars. Microwave reactions were performed with a Biotage Initiator Series Microwave (fixed hold time setting; reaction temperatures monitored by the internal infrared sensor).

Reactions were monitored by thin layer chromatography (TLC) on precoated TLC glass plates (silica gel 60 F254, 250 μ m thickness) or by LC/MS (30 mm \times 2 mm 2 μ m column + guard; 2 μ L injection; 3–98% MeCN/H₂O + 0.05% TFA gradient over 2.3 min; 0.9 mL/min flow; ESI; positive ion mode; UV detection at 254 nM). Visualization of the developed TLC chromatogram was performed by fluorescence quenching. Flash chromatography was performed on an automated purification system using prepacked silica gel columns. ¹H NMR were recorded on either a 500 or 600 MHz Varian spectrometer; chemical shifts (δ) are reported relative to residual protio solvent signals. Data for NMR spectra are reported as follows: chemical shift (δ ppm), multiplicity (s = singlet, brs = broad singlet, d = doublet, t = triplet, q = quartet, dd = doublet of doublets, m = multiplet), coupling constant (Hz), integration.

All compounds reported are of at least 95% purity, as judged by LCAP (150 mm \times 4.6 mm ID, 5 μ m column; 5 μ L injection; 10–100% MeCN/H₂O + 0.05% TFA gradient over 6.75 min; 1 mL/min flow; ESI; positive ion mode; UV detection at 254 nM, Bw8), with the exception of **56** (described in Supporting Information).

General Procedure for Formation of the Tricyclic Core. 7-Bromo-3-chloro-5H-benzo[4,5]cyclohepta[1,2-b]pyridin-5-one (3a). To a solution of methyl 5-chloro-2-methylnicotinate (3.50 g, 18.8 mmol) and *p*-bromobenzaldehyde (3.50 g, 18.8 mmol) in 500 mL of hexanes at 0 °C was added KO^t-Bu (1.0 M in THF; 37.6 mL, 37.6 mmol). The mixture was warmed to ambient temperature and THF (150 mL) was added. The mixture was stirred at ambient temperature overnight. The mixture was concentrated in vacuo to afford an orange–yellow solid. The solid was slurried in H₂O (50 mL) and 6 N aqueous HCl (30 mL). EtOH (100 mL) was added to the mixture. The solid was collected by filtration to afford 3.31 g of **4a** (52%). ¹H NMR (600 MHz, DMSO) δ 13.79 (br s, 1H), 8.76 (d, *J* = 2.4 Hz, 1H), 8.22 (d, *J* = 3.0 Hz, 1H), 8.02 (d, *J* = 15.6 Hz, 1H), 7.79 (d, *J* = 15.6 Hz, 1H), 7.61–7.54 (m, 4H). LRMS (ESI) calcd for (C₁₄H₁₀⁸¹BrClNO₂) [M + H]⁺ 340.0; found 339.9.

A flask was charged with **4a** (35 g, 93 mmol) and 350 mL of polyphosphoric acid (PPA). The mixture was heated to 200 °C overnight. The mixture was cooled to ambient temperature and then diluted in ice. Solid NaOH was added to adjust to pH >10. The mixture was diluted in DCM (8 L), Celite was added, and the mixture was stirred at ambient temperature for 30 min. The solid was removed by filtration, washing with DCM (4 L). The organic layer was separated and dried over MgSO₄. The solution was concentrated in vacuo to afford 10.4 g of **3a** as a brown solid (35%). ¹H NMR (600 MHz, DMSO) δ 8.98 (s, 1H), 8.42 (s, 1H), 8.19 (s, 1H), 8.00 (d, *J* = 7.8 Hz, 1H), 7.77 (d, *J* = 8.4 Hz,

1H), 7.44 (d, *J* = 12 Hz, 1H), 7.32 (d, *J* = 12.6 Hz, 1H). LRMS (ESI) calcd for (C₁₄H₈BrClNO) [M + H]⁺ 318.9; found 321.0.

General Procedure for the Conversion of 7-Bromo to 7-Amino Analogues. 7-Amino-3-chloro-5H-benzo[4,5]cyclohepta[1,2-b]pyridin-5-one (7). *Method A.* A dry flask was charged with **3a** (3.0 g, 9.4 mmol), Pd₂(dba)₃ (43 mg, 0.047 mmol), *rac*-BINAP (88 mg, 0.14 mmol), NaO^t-Bu (1.1 g, 11 mmol), 2,4-dimethoxybenzylamine (1.4 mL, 9.4 mmol), and 1,4-dioxane (100 mL). The mixture was sparged with argon for 10 min and then heated to 100 °C for 2 h. The reaction mixture was cooled to ambient temperature and concentrated in vacuo to afford a black oil. The black oil was slurried in MeOH (20 mL) and DCM (80 mL). Heptane (300 mL) was added to the mixture dropwise via addition funnel, and the mixture was stirred overnight. The resulting solid was collected by filtration to afford 2.6 g of **8** (68%). ¹H NMR (600 MHz, DMSO) δ 8.91–8.89 (m, 1H), 8.48–8.46 (m, 1H), 7.54 (d, *J* = 8.4 Hz, 1H), 7.39 (s, 1H), 7.29 (d, *J* = 12.6 Hz, 1H), 7.11 (d, *J* = 7.8 Hz, 1H), 7.09–7.04 (m, 2H), 7.01 (d, *J* = 12.6 Hz, 1H), 6.58–6.56 (m, 1H), 6.46–6.43 (m, 1H), 4.25 (d, *J* = 5.4 Hz, 2H), 3.82 (s, 3H), 3.70 (s, 3H). LRMS (ESI) calcd for (C₂₃H₂₀ClN₂O₃) [M + H]⁺ 407.1; found 407.0.

To a solution of **8** (50 mg, 0.12 mmol) in MeOH (1 mL) and DCM (5 mL) was added TFA (1 mL). The reaction mixture was stirred at 40 °C for 1 h. The reaction mixture was cooled to ambient temperature. The mixture was diluted in EtOAc and washed with saturated aqueous sodium bicarbonate. The organic layer was separated and dried over MgSO₄. The solution was concentrated in vacuo and purified by flash column chromatography (0–20% MeOH/DCM gradient) to afford 30 mg of **7** (95%).

Method B. A flask was charged with **3a** (1.05 g, 3.30 mmol), Pd₂(dba)₃ (8.0 mg, 0.008 mmol), *rac*-BINAP (15.0 mg, 0.025 mmol), NaO^t-Bu (0.444 g, 4.62 mmol), benzophenone imine (0.662 mL, 3.95 mmol), and toluene (40 mL). The mixture was sparged with argon for 10 min then heated to 110 °C for 2.5 h. The reaction mixture was cooled to ambient temperature and concentrated in vacuo. The solid was dissolved in 6N HCl(aq) (1 mL) and THF (20 mL) and allowed to stir at ambient temperature for 2 h. The mixture was diluted in EtOAc (300 mL) and washed with saturated aqueous sodium bicarbonate (100 mL) and H₂O (200 mL). The organic layer was separated and dried over MgSO₄. The solution was concentrated in vacuo and purified by flash column chromatography (0–30% EtOAc/DCM gradient) to afford 700 mg of **7** (83%). ¹H NMR (600 MHz, DMSO) δ 8.91 (d, *J* = 3.0 Hz, 1H), 8.48 (d, *J* = 3.0 Hz, 1H), 7.52 (d, *J* = 10.8 Hz, 1H), 7.42 (d, *J* = 3.6 Hz, 1H), 7.30 (d, *J* = 14.4 Hz, 1H), 7.03–6.99 (m, 2H), 6.17 (s, 2H). LRMS (ESI) calcd for (C₁₄H₁₀ClN₂O) [M + H]⁺ 257.0; found 257.0.

General Procedure for the Incorporation of Sulfonamides. N-(3-Chloro-5-oxo-5H-benzo[4,5]cyclohepta[1,2-b]pyridin-7-yl) methanesulfonamide (12a). *Method A.* To a solution of **7** (0.70 g, 2.7 mmol) and triethylamine (0.83 mL, 5.9 mmol) in EtOAc (40 mL) at 0 °C was added methanesulfonyl chloride (0.42 mL, 5.4 mmol). The reaction mixture was allowed to warm to ambient temperature and stirred for 1 h. The mixture was diluted in EtOAc and washed with saturated aqueous sodium bicarbonate and H₂O. The organic layer was separated and dried over MgSO₄. The solution was concentrated in vacuo to afford a yellow solid. The yellow solid was dissolved in MeOH (150 mL) and 5N NaOH(aq) (5 mL) and allowed to stir for 1 h. The mixture was concentrated in vacuo to ~10 mL. The mixture was diluted in EtOAc (250 mL) and washed with saturated aqueous NH₄Cl and H₂O. The organic layer was separated and dried over MgSO₄. The solution was concentrated in vacuo to afford 0.84 g of **12a** (93%).

Method B. A flask was charged with **7** (5.00 g, 15.7 mmol), methanesulfonamide (1.49 g, 15.7 mmol), Pd₂(dba)₃ (0.714 g, 0.780 mmol), Xantphos (1.36 g, 2.35 mmol), Cs₂CO₃ (15.3 g, 47.0 mmol), and 1,4-dioxane (100 mL). The mixture was sparged with argon for 10 min and then heated to 95 °C overnight. The reaction mixture was cooled to ambient temperature and then diluted in EtOAc (2 L) and

washed with H₂O (1 L). The organic layer was separated, washed with brine (500 mL), and dried over MgSO₄. The solution was concentrated in vacuo to afford a crude solid that was dissolved in 3:1 hot DCM/MeOH (150 mL) and stirred for 2 h. Hexanes (150 mL) was added dropwise via addition funnel, and the mixture was allowed to stir overnight. Additional hexanes (50 mL) was added. After stirring for 4 h, the solids were collected by filtration to afford 3.65 g of **12a** (70%). ¹H NMR (600 MHz, DMSO) δ 10.42 (s, 1H), 8.97 (dd, *J* = 2.4 Hz, 1.2 Hz, 1H), 8.48 (d, *J* = 2.4 Hz, 1H), 8.00 (d, *J* = 2.4 Hz, 1H), 7.80 (d, *J* = 7.8 Hz, 1H), 7.62 (dd, *J* = 8.4, 2.4 Hz, 1H), 7.42 (d, *J* = 12.0 Hz, 1H), 7.23 (d, *J* = 12.0 Hz, 1H), 3.09 (s, 3H). LRMS (ESI) calcd for (C₁₅H₁₂ClN₂O₃S) [M + H]⁺ 335.0; found 335.1.

N-(5-Oxo-3-phenyl-5H-benzo[4,5]cyclohepta[1,2-b]pyridin-7-yl)methanesulfonamide (1). Compound **3b** (200 mg, 0.552 mmol), methanesulfonamide (57.8 mg, 0.607 mmol), Pd₂dba₃ (25.3 mg, 0.028 mmol), Xantphos (47.9 mg, 0.083 mmol), and Cs₂CO₃ (540 mg, 1.656 mmol) were combined in 1,4-dioxane (5.5 mL) and sparged with argon for 10 min. The reaction mixture was heated to 100 °C and stirred for 2 h then cooled to ambient temperature. The reaction mixture was diluted in EtOAc, washed with saturated aqueous sodium bicarbonate and brine, and then dried over sodium sulfate, filtered, and concentrated. The residue was purified by reverse phase HPLC (CH₃CN/H₂O with 0.1% TFA). The fractions containing product were combined and diluted in EtOAc (200 mL) and aqueous sodium bicarbonate (100 mL) and heated to 70 °C so that all of the solids went into solution. The layers were separated, the organic layer was washed with brine, and then the combined aqueous layers were back-extracted with EtOAc. The combined organic layers were dried over sodium sulfate. The solution was filtered and concentrated under reduced pressure to give 136 mg of compound **1** (65%) as a yellow solid. ¹H NMR (600 MHz, DMSO-*d*₆) δ 10.42 (br s, 1H), 9.24 (s, 1H), 8.64 (s, 1H), 8.03 (s, 1H), 7.85 (s, 1H), 7.83 (s, 1H), 7.78 (d, *J* = 8.4 Hz, 1H), 7.61 (d, *J* = 8.4 Hz, 1H), 7.53–7.49 (m, 2H), 7.46–7.42 (m, 1H), 7.38 (d, *J* = 12.6 Hz, 1H), 7.26 (d, *J* = 12.0 Hz, 1H), 3.09 (s, 3H). LRMS (ESI) calcd for (C₂₁H₁₇N₂O₃S) [M + H]⁺ 377.1; found 377.1.

General Procedure for the Incorporation of Amines: N-[3-(4-Isopropylpiperazin-1-yl)-5-oxo-5H-benzo[4,5]cyclohepta[1,2-b]pyridin-7-yl)methanesulfonamide (34). A flask was charged with **12a** (50 mg, 0.15 mmol), 4-dimethylamino-piperidine (38 mg, 0.30 mmol), Pd₂(dba)₃ (1.5 mg, 0.002 mmol), *rac*-BINAP (3.0 mg, 0.005 mmol), NaOt-Bu (43 mg, 0.45 mmol), and 1,4-dioxane (3 mL). The mixture was sparged with argon for 10 min and then heated to 105 °C overnight. The reaction mixture was cooled to ambient temperature, diluted in EtOAc, and washed with H₂O and saturated aqueous NH₄Cl. The organic layer was separated and dried over MgSO₄. The solution was concentrated in vacuo and purified by reverse phase HPLC (20–100% CH₃CN/H₂O with 0.1% TFA) to afford 15 mg (24%) of **34**. ¹H NMR (600 MHz, DMSO-*d*₆) δ 10.28 (s, 1H), 8.76 (d, *J* = 3.0 Hz, 1H), 8.01 (d, *J* = 2.4 Hz, 1H), 7.79 (d, *J* = 3.0 Hz, 1H), 7.73 (d, *J* = 9.0 Hz, 1H), 7.57 (dd, *J* = 8.4, 2.4 Hz, 1H), 7.20–7.14 (m, 2H), 3.38–3.34 (m, 4H), 3.05 (s, 3H), 2.72 (m, 1H), 2.62–2.56 (bs, 4H), 0.99 (d, *J* = 7.2 Hz, 6H). LRMS (ESI) calcd for (C₂₂H₂₇N₄O₃S) [M + H]⁺ 427.2; found 427.2.

Compound **14** was isolated as a side-product from this reaction. ¹H NMR (600 MHz, DMSO-*d*₆) δ 8.92–8.90 (m, 1H), 8.45 (d, *J* = 7.8 Hz, 1H), 7.97 (d, *J* = 2.4 Hz, 1H), 7.78 (d, *J* = 8.4 Hz, 1H), 7.62–7.58 (m, 2H), 7.39 (d, *J* = 12.6 Hz, 1H), 7.23 (d, *J* = 12.6 Hz, 1H), 3.06 (s, 3H). LRMS (ESI) calcd for (C₁₅H₁₃N₂O₃S) [M + H]⁺ 301.1; found 301.1.

N-[3-(2-Chlorophenyl)-5-oxo-5H-benzo[4,5]cyclohepta[1,2-b]pyridin-7-yl)methanesulfonamide (37). A reaction vessel was charged with **12a** (40.0 mg, 0.12 mmol), 2-chlorophenylboronic acid (22 mg, 0.14 mmol), Pd(PPh₃)₄ (4.0 mg, 0.004 mmol), K₂CO₃ (50 mg, 0.36 mmol), and 1,4-dioxane (3 mL). The mixture was sparged

with argon for 10 min and then heated to 100 °C overnight. The reaction mixture was cooled to ambient temperature. The mixture was diluted in EtOAc and washed with H₂O and saturated aqueous NH₄Cl. The organic layer was separated and dried over MgSO₄. The solution was filtered, concentrated in vacuo, and purified by reverse phase HPLC (40–100% CH₃CN/H₂O with 0.05% TFA) to afford 35 mg of **37** (71%). ¹H NMR (600 MHz, DMSO-*d*₆) δ 10.40 (s, 1H), 9.03 (d, *J* = 1.8 Hz, 1H), 8.51 (d, *J* = 2.4 Hz, 1H), 8.02 (d, *J* = 2.4 Hz, 1H), 7.83 (d, *J* = 8.4 Hz, 1H), 7.66–7.58 (m, 3H), 7.52–7.48 (m, 2H), 7.46 (d, *J* = 12.0 Hz, 1H), 7.31 (d, *J* = 12.0 Hz, 1H), 3.09 (s, 3H). LRMS (ESI) calcd for (C₂₁H₁₆ClN₂O₃S) [M + H]⁺ 411.1; found 411.0.

N-(3-Isothiazol-4-yl-5-oxo-5H-benzo[4,5]cyclohepta[1,2-b]pyridin-7-yl)methanesulfonamide (45). *Step 1.* A flask was charged with **12a** (1.12 g, 3.34 mmol), bis(pinacolato)diboron (1.36 g, 5.35 mmol), Pd₂(dba)₃ (0.160 g, 0.170 mmol), tricyclohexylphosphine (0.120 g, 0.400 mmol), potassium acetate (0.820 g, 8.35 mmol), and 1,4-dioxane (50 mL). The mixture was sparged with argon for 10 min and then heated to 100 °C overnight. The reaction mixture was cooled to ambient temperature. The mixture was diluted in EtOAc and washed with saturated aqueous sodium bicarbonate. The organic layer was separated and dried over MgSO₄. The solution was filtered, concentrated in vacuo, and purified by reverse phase HPLC (10–100% CH₃CN/H₂O with 0.1% TFA). The fractions were diluted in EtOAc (500 mL) and washed with saturated aqueous sodium bicarbonate (100 mL). The organic layer was separated, dried over MgSO₄, and filtered and concentrated in vacuo to afford 0.600 g of {7-[(methylsulfonyl)amino]-5-oxo-5H-benzo[4,5]cyclohepta[1,2-b]pyridin-3-yl}boronic acid (52%). ¹H NMR (600 MHz, CDCl₃) δ 9.16 (d, *J* = 1.8 Hz, 1H), 8.88 (d, *J* = 1.8 Hz, 1H), 7.91 (d, *J* = 2.4 Hz, 1H), 7.68 (dd, *J* = 7.8, 3.0 Hz, 1H), 7.61 (d, *J* = 7.8 Hz, 1H), 7.35 (d, *J* = 12.0 Hz, 1H), 7.28–7.21 (m, 2H), 3.08 (s, 3H). LRMS (ESI) calcd for (C₁₅H₁₄BN₂O₅S) [M + H]⁺ 345.1; found 345.1.

Step 2. A reaction vessel was charged with {7-[(methylsulfonyl)amino]-5-oxo-5H-benzo[4,5]cyclohepta[1,2-b]pyridin-3-yl}boronic acid (50 mg, 0.15 mmol), 4-bromo-isothiazole (48 mg, 0.29 mmol), Pd(PPh₃)₄ (5.0 mg, 0.004 mmol), K₂CO₃ (60 mg, 0.44 mmol), and DMF (2 mL). The mixture was sparged with argon for 10 min then placed in the microwave reactor and heated to 185 °C for 20 min. The reaction mixture was cooled to ambient temperature. The mixture was diluted in EtOAc and washed with saturated aqueous NH₄Cl. The organic layer was separated and dried over MgSO₄. The solution was filtered, concentrated in vacuo, and purified by reverse phase HPLC (20–100% CH₃CN/H₂O with 0.1% TFA) to afford 11 mg of **45** (20%). ¹H NMR (600 MHz, DMSO-*d*₆) δ 10.62–10.18 (bs, 1H), 9.70 (s, 1H), 9.38 (d, *J* = 1.8 Hz, 1H), 9.26 (s, 1H), 8.78 (d, *J* = 2.4 Hz, 1H), 8.00 (d, *J* = 2.4 Hz, 1H), 7.78 (d, *J* = 8.4 Hz, 1H), 7.59 (dd, *J* = 8.4, 2.4 Hz, 1H), 7.39 (d, *J* = 12.0 Hz, 1H), 7.26 (d, *J* = 12.6 Hz, 1H), 3.08 (s, 3H). LRMS (ESI) calcd for (C₁₈H₁₄N₃O₃S₂) [M + H]⁺ 384.0; found 384.0.

N,N-Dimethyl-N'-[3-(1-methyl-1H-pyrazol-4-yl)-5-oxo-5H-benzo[4,5]cyclohepta[1,2-b]pyridin-7-yl]sulfuric Diamide (59). *Step 1.* *N'*-(3-Dihloro-5-oxo-5H-benzo[4,5]cyclohepta[1,2-b]pyridin-7-yl)-*N,N*-dimethylsulfuric Diamide (**13a**). Compound **3a** (11.93 g, 37.21 mmol) and *N,N*-dimethylsulfuric diamide (4.62 g, 37.2 mmol) were combined in 1,4-dioxane (350 mL), and the solution was sparged with argon for 1 h. Pd₂dba₃ (1.70 g, 1.86 mmol), Xantphos (3.23 g, 5.58 mmol), and Cs₂CO₃ (36.37 g, 111.6 mmol) were added, and the reaction mixture was sparged with argon for an additional 30 min. The reaction was then heated to 100 °C for 2 h, during which time a thick precipitate formed. After cooling to ambient temperature, the reaction mixture was diluted in EtOAc (1.5 L) and washed with saturated aqueous sodium bicarbonate (2 × 300 mL) and brine (300 mL). The combined aqueous layers were filtered through a pad of Celite, and the Celite pad was washed with EtOAc (500 mL). The aqueous layer was combined with this Celite EtOAc wash in a separatory funnel and then further washed with 300 mL of EtOAc. The combined organic layers were dried over sodium

sulfate and then filtered and concentrated in vacuo to give a brown solid. This solid was dissolved in boiling 10% MeOH/DCM (800 mL), and then hexanes were slowly added (500 mL) until a precipitate began to form from the stirring solution. The mixture was allowed to cool to ambient temperature, and then additional hexanes (3×250 mL aliquots at 30 min intervals) were added and the mixture was left to stand for an additional 1 h. The solids were collected by filtration and dried under vacuum to afford 8.10 g of compound **13a** (60%). If desired, additional **13a** could be recovered from the mother liquor via flash column chromatography. ^1H NMR (600 MHz, DMSO- d_6) δ 10.55 (s, 1H), 8.96 (d, $J = 2.4$ Hz, 1H), 8.49 (d, $J = 2.9$ Hz, 1H), 7.99 (d, $J = 2.4$ Hz, 1H), 7.77 (d, $J = 8.5$ Hz, 1H), 7.60 (dd, $J = 8.5, 2.6$ Hz, 1H), 7.40 (d, $J = 12.6$ Hz, 1H), 7.21 (d, $J = 12.3$ Hz, 1H), 2.72 (s, 6H). LRMS (ESI) calcd for ($\text{C}_{16}\text{H}_{15}\text{ClN}_3\text{O}_3\text{S}$) [$\text{M} + \text{H}$] $^+$ 364.0; found 364.1.

Step 2. A flask was charged with compound **13a** (1.22 g, 3.35 mmol), 1-methyl-4-(4,4,5,5-tetramethyl-1,3,2-dioxaborolan)-1H-pyrazole (2.09 g, 10.1 mmol), tri-*t*-butylphosphonium tetrafluoroborate (97.0 mg, 0.334 mmol), $\text{Pd}_2(\text{dba})_3$ (154 mg, 0.168 mmol), KF (643 mg, 11.1 mmol), and DMF (40 mL). The mixture was sparged with argon for 10 min and then heated to 100 °C for 2 h. The reaction mixture was cooled to ambient temperature and then diluted in EtOAc (500 mL) and washed with H_2O (2×100 mL). The organic layer was separated and dried over MgSO_4 . The solution was concentrated in vacuo to afford a yellow solid. The yellow solid was recrystallized from 1:4:4 MeOH/DCM/hexanes to afford 1.01 g of **59** (74%). ^1H NMR (600 MHz, DMSO- d_6) δ 10.52 (s, 1H), 9.20 (d, $J = 2.4$ Hz, 1H), 8.57 (d, $J = 1.8$ Hz, 1H), 8.47 (s, 1H), 8.14 (s, 1H), 8.00 (d, $J = 2.4$ Hz, 1H), 7.75 (d, $J = 8.4$ Hz, 1H), 7.57 (dd, $J = 8.4, 2.4$ Hz, 1H), 7.32 (d, $J = 12.6$ Hz, 1H), 7.23 (d, $J = 12.0$ Hz, 1H), 3.88 (s, 3H), 2.73 (s, 6H). LRMS (ESI) calcd for ($\text{C}_{20}\text{H}_{20}\text{N}_5\text{O}_3\text{S}$) [$\text{M} + \text{H}$] $^+$ 410.1; found 410.1.

Benzyl [(2R)-1,4-Dioxan-2-ylmethyl]methylcarbamate.
Step 1. 1-(1,4-Dioxan-2-yl)-*N*-methylmethanamine (10.2 g, 78.0 mmol) was dissolved in 200 mL of DCM. Benzyl chloridocarbonate (16.4 mL, 117 mmol) and triethylamine (32.6 mL, 234 mmol) were added, and the solution was stirred at ambient temperature. After 12 h, the solution was concentrated and then diluted with EtOAc (1 L) and washed with saturated aqueous sodium bicarbonate (100 mL) and H_2O (100 mL). The organic layer was separated, dried with magnesium sulfate, filtered, concentrated in vacuo, and purified by flash column chromatography (0–100% EtOAc/hexanes gradient) to afford 19.0 g of racemic benzyl (1,4-dioxan-2-ylmethyl)methylcarbamate (92% yield).

The racemic mixture was dissolved in 75 mL of heptane and 25 mL of isopropyl alcohol. The material was resolved on a chiral AD column (15% isopropyl alcohol/heptane) to afford 8.4 g of enantiomer A [τ_{R} : 9.35 min (analytical chiral HPLC, AD column, 0.46 cm \times 25 cm id, 15% isopropyl alcohol/heptane, isocratic, flow rate = 0.75 mL/min)] and 8.4 g of enantiomer B [τ_{R} : 10.92 min (analytical chiral HPLC, AD column, 0.46 cm \times 25 cm id, 15% isopropyl alcohol/heptane, isocratic, flow rate = 0.75 mL/min)].

^1H NMR (600 MHz, DMSO- d_6) δ 7.36–7.32 (m, 4H), 7.30–7.27 (m, 1H), 5.03 (s, 2H), 3.72–3.56 (m, 4H), 3.54–3.46 (m, 1H), 3.44–3.38 (m, 1H), 3.26–3.10 (m, 3H), 2.90–2.84 (m, 3H). LRMS (ESI) calcd for ($\text{C}_{14}\text{H}_{20}\text{NO}_4$) [$\text{M} + \text{H}$] $^+$ 266.1; found 266.2.

The absolute stereochemistry of enantiomer A and B was determined by comparison of HPLC retention times to benzyl [(2S)-1,4-dioxan-2-ylmethyl]methylcarbamate, which was prepared from commercially available (2R)-3-(benzyloxy)propane-1,2-diol as described in the Supporting Information.

***N*-[(2R)-1,4-Dioxan-2-ylmethyl]-*N*-methylsulfuric Diamide.**
Step 1. Benzyl [(2R)-1,4-dioxan-2-ylmethyl]methylcarbamate (enantiomer A, 8.4 g, 31.7 mmol) was dissolved in dry ethanol (200 mL) under a nitrogen atmosphere, and then 10% (w/w) palladium on carbon (0.84 g, 0.79 mmol) and 10 N HCl (6.4 mL) were added. The flask was placed

under an atmosphere of hydrogen (balloon) and stirred vigorously. After 3 h, the solution was filtered through Celite, concentrated in vacuo, and azeotroped with toluene to afford the crude residue. The residue was dissolved in 4.0 M HCl in 1,4-dioxane (20 mL) and concentrated in vacuo to afford 5.37 g of 1-[(2R)-1,4-dioxan-2-yl]-*N*-methylmethanamine hydrochloride (100%). ^1H NMR (600 MHz, DMSO- d_6): δ 8.94 (s, 1H), 8.75 (s, 1H), 3.86–3.80 (m, 1H), 3.76 (d, $J = 11.6$ Hz, 1H), 3.70 (d, $J = 11.5$ Hz, 1H), 3.64 (d, $J = 11.6$ Hz, 1H), 3.58 (dt, $J = 11.3, 2.3$ Hz, 1H), 3.45 (dt, $J = 11.2, 2.4$ Hz, 1H), 3.22 (t, $J = 10.6$ Hz, 1H), 2.97–2.91 (m, 1H), 2.91–2.85 (m, 1H), 2.50 (d, $J = 5.2, 3\text{H}$).

Step 2. 1-[(2R)-1,4-Dioxan-2-yl]-*N*-methylmethanamine hydrochloride (5.37 g, 32.1 mmol), *N*-[1-[(*tert*-butoxycarbonyl)amino]sulfonyl]pyridin-4(1H)-ylidene]-*N*-methylmethanaminium (9.7 g, 32.1 mmol), and triethylamine (5.4 mL, 39 mmol) were slurried in DCM (200 mL) and stirred at ambient temperature. After 4 h, the solution was concentrated in vacuo and purified by flash column chromatography (0–75% EtOAc/hexanes gradient) to afford 8.81 g of *tert*-butyl {[(2R)-1,4-dioxan-2-ylmethyl](methylamino)sulfonyl}carbamate (88%). ^1H NMR (600 MHz, DMSO- d_6) δ 10.93 (s, 1H), 3.72–3.68 (m, 1H), 3.66–3.63 (m, 2H), 3.62–3.58 (m, 1H), 3.55–3.50 (m, 1H), 3.44–3.39 (m, 1H), 3.21–3.14 (m, 3H), 2.81 (s, 3H), 1.39 (s, 9H). LRMS (ESI) calcd for ($\text{C}_{11}\text{H}_{22}\text{N}_2\text{O}_6\text{SNa}$) [$\text{M} + \text{Na}$] $^+$ 333.1; found 333.1.

Step 3. *tert*-Butyl {[(2R)-1,4-dioxan-2-ylmethyl](methylamino)sulfonyl}carbamate (8.81 g, 28.4 mmol) was dissolved in DCM (100 mL) and trifluoroacetic acid (100 mL) and stirred at ambient temperature. After 6 h, the solution was concentrated and azeotroped twice with heptane to afford 8.35 g of {[(2R)-1,4-dioxan-2-ylmethyl](methylamino)sulfonyl}ammonium trifluoroacetate (91%). ^1H NMR (600 MHz, DMSO- d_6) δ 6.70 (s, 2H), 3.72–3.63 (m, 3H), 3.62–3.58 (m, 1H), 3.56–3.50 (m, 1H), 3.44–3.39 (m, 1H), 3.21–3.16 (m, 1H), 2.90–2.86 (m, 2H), 2.65 (s, 3H). LRMS (ESI) calcd for ($\text{C}_6\text{H}_{15}\text{N}_2\text{O}_4\text{S}$) [$\text{M} + \text{H}$] $^+$ 211.1; found 211.1.

***N*-[(2R)-1,4-Dioxan-2-ylmethyl]-*N*-methyl-*N'*-[3-(1-methyl-1H-pyrazol-4-yl)-5-oxo-5H-benzo[4,5]cyclohepta[1,2-*b*]pyridin-7-yl]sulfuric Diamide (81).**⁵⁵
Step 1. Compound **7** (9.1 g, 28.3 mmol), {[(2R)-1,4-dioxan-2-ylmethyl](methylamino)sulfonyl}ammonium trifluoroacetate (8.35 g, 25.8 mmol), Pd_2dba_3 (1.18 g, 1.29 mmol), Xantphos (2.24 g, 3.87 mmol), Cs_2CO_3 (33.6 g, 103 mmol), and 1,4-dioxane (300 mL) were combined in a dry flask. Argon was sparged through the mixture for 5 min, and then the mixture was heated to 95 °C. After 3 h, the solution was concentrated in vacuo, diluted with EtOAc (1.5 L), and washed with H_2O (500 mL) and brine (500 mL). The organic layer was isolated, dried with magnesium sulfate, filtered, concentrated in vacuo, and purified by flash column chromatography (0–100% EtOAc/hexanes gradient) to afford 9.95 g of *N'*-(3-chloro-5-oxo-5H-benzo[4,5]cyclohepta[1,2-*b*]pyridin-7-yl)-*N*-[(2R)-1,4-dioxan-2-ylmethyl]-*N*-methylsulfuric diamide (86%). ^1H NMR (600 MHz, DMSO- d_6) δ 10.57 (s, 1H), 8.97 (d, $J = 2.4$ Hz, 1H), 8.49 (d, $J = 2.4$ Hz, 1H), 7.96 (d, $J = 2.4$ Hz, 1H), 7.78 (d, $J = 8.4$ Hz, 1H), 7.57 (dd, $J = 8.4, 2.4$ Hz, 1H), 7.41 (d, $J = 12.6$ Hz, 1H), 7.22 (d, $J = 12.6$ Hz, 1H), 3.65–3.60 (m, 2H), 3.59–3.52 (m, 2H), 3.45–3.40 (m, 1H), 3.38–3.33 (m, 1H), 3.15–3.10 (m, 3H), 2.77 (s, 3H). LRMS (ESI) calcd for ($\text{C}_{20}\text{H}_{21}\text{ClN}_3\text{O}_5\text{S}$) [$\text{M} + \text{H}$] $^+$ 450.1; found 450.1.

Step 2. *N'*-(3-Chloro-5-oxo-5H-benzo[4,5]cyclohepta[1,2-*b*]pyridin-7-yl)-*N*-[(2R)-1,4-dioxan-2-ylmethyl]-*N*-methylsulfuric diamide (8.05 g, 17.9 mmol), 1-methyl-4-(4,4,5,5-tetramethyl-1,3,2-dioxaborolan-2-yl)-1H-pyrazole (11.2 g, 53.7 mmol), $\text{Pd}_2(\text{dba})_3$ (0.820 g, 0.895 mmol), *t*-Bu₃PHF₄ (0.520 g, 1.79 mmol), potassium fluoride (3.43 g, 59.1 mmol), and DMF (200 mL) were combined in a dry flask. The mixture was sparged with argon for 5 min and then heated to 100 °C. After 3 h, the solution was diluted with EtOAc and washed with saturated sodium bicarbonate, H_2O , and brine. The organic layer was dried with magnesium sulfate, filtered, and concentrated in vacuo. The residue was crystallized from a mixture of methanol (70 mL), DCM (275 mL), and hexanes

(600 mL) to afford 6.17 g of *N*-[(2*R*)-1,4-dioxan-2-ylmethyl]-*N*-methyl-*N*'-[3-(1-methyl-1*H*-pyrazol-4-yl)-5-oxo-5*H*-benzo[4,5]cyclohepta[1,2-*b*]pyridin-7-yl]sulfuric diamide (70%). ¹H NMR (600 MHz, DMSO-*d*₆) δ 10.53 (s, 1H), 9.19 (d, *J* = 1.8 Hz, 1H), 8.56 (d, *J* = 2.4 Hz, 1H), 8.46 (s, 1H), 8.13 (s, 1H), 7.96 (d, *J* = 2.4 Hz, 1H), 7.75 (d, *J* = 9.0 Hz, 1H), 7.55 (dd, *J* = 8.4, 2.4 Hz, 1H), 7.32 (d, *J* = 12.6 Hz, 1H), 7.23 (d, *J* = 12.6 Hz, 1H), 3.88 (s, 3H), 3.65–3.60 (m, 2H), 3.59–3.51 (m, 2H), 3.45–3.40 (m, 1H), 3.38–3.33 (m, 1H), 3.15–3.10 (m, 3H), 2.78 (s, 3H). LRMS (ESI) calcd for (C₂₄H₂₆N₅O₅S) [M + H]⁺ 496.2; found 496.1.

In Vitro Kinase Assays. As described in ref 31, *c*-Met-catalyzed phosphorylation of *N*-biotinylated peptide (EQEPEPEGDYFEWLE-CONH₂) was measured using a time-resolved fluorescence resonance energy transfer assay. To evaluate kinase selectivity, a single concentration (1 μmol/L) of **81** was tested using 216 kinases by Upstate Biotechnology, Inc. (Millipore), which also determined the IC₅₀ for DRAK1, DYRK2, IRAK1, IRAK4, MELK, and MLK1. The IC₅₀ for Ron, Mer, Flt1, Flt3, Flt4, KDR, PDGFRβ, FGFR1, FGFR2, FGFR3, TrkA, and TrkB were determined using time-resolved fluorescence resonance energy transfer assays similar to the *c*-Met kinase assay.

Cellular Assays. As described in ref 31, proliferation and viability of tumor cells was measured using the ViaLight PLUS kit (Cambrex). Analysis of phosphorylation status of *c*-Met, in cells: Tumor cells were treated for 2 h with **81** or vehicle in RPMI 1640 supplemented with 10% fetal bovine serum and 10 mmol/L HEPES. When called for, the cells were stimulated with HGF or EGF during the last 10 min of the 2 h incubation. The cells were lysed with a denaturing or nondenaturing buffer containing phosphatase and protease inhibitors and subjected to Western blot or immunoprecipitation–Western blot analysis.

Tumor Xenograft Models. As described in ref 31, GTL-16 cells were inoculated sc into the flank of female nude CD-1 nu/nu mice. When mean tumor size reached a predetermined range, the mice were randomized and given vehicle or **81** by po gavage once or twice daily. Tumor volumes were determined using calipers. The percentage increase in the volume of a xenograft tumor on day *n* versus day 0 (the day when dosing of **81** began) was calculated as (tumor volume on day *n* – tumor volume on day 0)/tumor volume on day 0 × 100. The mean percentage of tumor growth inhibition in each **81**-treated group relative to the vehicle-treated group was calculated as (1 – mean percent increase of tumor volume in the **81**-treated group/mean percent increase of the tumor volume in the vehicle-treated group) × 100.

Measurement of *c*-Met (Y1349) Phosphorylation in Xenograft Tumors. As described in ref 31, mice bearing GTL-16 tumors were euthanized 1 h after po administration of **81**. The tumors were excised, snap-frozen, and dispersed using a Qiagen Tissue-Lyser in a nondenaturing lysis buffer containing protease and phosphatase inhibitors. The homogenate was lysed at 4 °C for 1 h, clarified by centrifugation, and then analyzed by quantitative Western blotting for phospho-*c*-Met (Y1349) and total *c*-Met. The pMet (Y1349) signal of each *c*-Met band was normalized with its total *c*-Met signal. To combine or compare data from several gels, the pY1349/total Met ratio for each *c*-Met band was further normalized to the average pY1349/total *c*-Met ratio of the vehicle-treated tumor samples on the same gel.

Crystallography. The crystal structure of the autophosphorylated *c*-Met kinase domain bound to **82** were determined as described previously.⁵⁰

■ ASSOCIATED CONTENT

Supporting Information. Full experimentals and ¹H NMR data are available for compounds **3b–e**, **10–11**, **21–29**, **30–33**, **35–36**, **38–44**, **46–58**, **60–80**, and **82** and structure-determination statistics for the crystal structure of the *c*-Met kinase domain complex with **82** are presented. This material is available free of charge via the Internet at <http://pubs.acs.org>.

Accession Codes

PDB ID 3R7O.

■ AUTHOR INFORMATION

Corresponding Author

*Phone: 617-992-2057. E-mail: jason_katz2@merck.com. Fax: 617-992-2403.

■ ACKNOWLEDGMENT

We thank Bruce Adams for assistance in NMR structural analysis and Regina Black for purification of key intermediates. In addition, we thank Elizabeth Stanton for analysis and compilation of analytical data.

■ ABBREVIATIONS USED

ATP, adenosine triphosphate; BINAP, 2,2'-bis(diphenylphosphino)-1,1'-binaphthyl; dba, dibenzylideneacetone; DCM, dichloromethane; DMF, *N,N*-dimethylformamide; DMSO, dimethylsulfoxide; dpfp, 1,1'-bis(diphenylphosphino)ferrocene; EtOAc, ethyl acetate; HGF, hepatocyte growth factor; HGFR, hepatocyte growth factor receptor; IP, intraperitoneal injection; iv, intravenous; Ms, methanesulfonyl; NMP, *N*-methylpyrrolidinone; PK, pharmacokinetic; PPA, polyphosphoric acid; SAR, structure–activity relationship; TBAF, tetrabutylammonium fluoride; Tf, trifluoromethanesulfonyl; TFA, trifluoroacetic acid; THF, tetrahydrofuran; Xantphos, 4,5-bis(diphenylphosphino)-9,9-dimethylxanthene

■ REFERENCES

- (1) Longati, P.; Bardelli, A.; Ponzetto, C.; Naldini, L.; Comoglio, P. M. Tyrosines1234–1235 are Critical for Activation of the Tyrosine Kinase Encoded by the MET Proto-oncogene (HGF Receptor). *Oncogene* **1994**, *9*, 49–57.
- (2) Birchmeier, C.; Birchmeier, W.; Gherardi, E.; Vande Woude, G. F. Met, Metastasis, Motility and More. *Nature Rev. Mol. Cell Biol.* **2003**, *4*, 915–925.
- (3) Benvenuti, S.; Comoglio, P. M. The MET Receptor Tyrosine Kinase in Invasion and Metastasis. *J. Cell. Physiol.* **2007**, *213*, 316–325.
- (4) Ponzetto, C.; Bardelli, A.; Zhen, Z.; Maina, F.; dalla Zonca, P.; Giordano, S.; Graziani, A.; Panayotou, G.; Comoglio, P. M. A Multifunctional Docking Site Mediates Signaling and Transformation by the Hepatocyte Growth Factor/Scatter Factor Receptor Family. *Cell* **1994**, *77*, 261–271.
- (5) Brinkmann, V.; Foroutan, H.; Sachs, M.; Weidner, K. M.; Birchmeier, W. Hepatocyte Growth Factor/Scatter Factor Induces a Variety of Tissue Specific Morphogenic Programs in Epithelial Cells. *J. Cell Biol.* **1995**, *131*, 1573–1586.
- (6) Bussolino, F.; Di Renzo, M. F.; Ziche, M.; Bocchietto, E.; Olivero, M.; Naldini, L.; Gaudina, G.; Tamagnone, L.; Coffer, A.; Comoglio, P. M. Hepatocyte Growth Factor is a Potent Angiogenic Factor Which Stimulates Endothelial Cell Motility and Growth. *J. Cell Biol.* **1992**, *119*, 629–641.
- (7) Gonzatti-Haces, M.; Seth, A.; Park, M.; Copeland, T.; Oroszlan, S.; Vande Woude, G. F. Characterization of the TPR-MET Oncogene p65 and the MET Protooncogene p140 Protein-Tyrosine Kinases. *Proc. Natl. Acad. Sci. U.S.A.* **1988**, *85*, 21–25.
- (8) Schmidt, L.; Duh, F. M.; Chen, F.; Kishida, T.; Glenn, G.; Choyke, P.; Scherer, S. W.; Zhuang, Z.; Lubensky, I.; Dean, M.; Allikmets, R.; Chidambaram, A.; Bergerheim, U. R.; Feltis, J. T.; Casadevall, C.; Zamarron, A.; Bernues, M.; Richard, S.; Lips, C. J. M.; Walther, M. M.; Tsui, L.-C.; Geil, L.; Orcutt, M. L.; Stackhouse, T.; Lipan, J.; Slife, L.; Brauch, H.; Decker, J.; Niehans, G.; Hughson, M. D.

Moch, H.; Storkel, S.; Lerman, M. I.; Linehan, W. M.; Zbar, B. Germline and Somatic Mutations in the Tyrosine Kinase Domain of the MET Proto-oncogene in Papillary Renal Carcinomas. *Nature Genet.* **1997**, *16*, 68–73.

(9) Jeffers, M.; Fiscella, M.; Webb, C. P.; Anver, M.; Koochekpour, S.; Vande Woude, G. F. The Mutationally Activated Met Receptor Mediates Motility and Metastasis. *Proc. Natl. Acad. Sci. U.S.A.* **1998**, *95*, 1441–1442.

(10) Christensen, J. G.; Burrows, J.; Salgia, R. c-Met as a Target for Human Cancer and Characterization of Inhibitors for Therapeutic Intervention. *Cancer Lett.* **2005**, *225*, 1–26.

(11) Smolen, G. A.; Sordella, R.; Muir, B.; Mohapatra, G.; Barmettler, A.; Archibald, H.; Kim, W. J.; Okimoto, R. A.; Bell, D. W.; Sgroi, D. C.; Christensen, J. G.; Settleman, J.; Haber, D. A. Amplification of MET May Identify a Subset of Cancers with Extreme Sensitivity to the Selective Tyrosine Kinase Inhibitor PHA-665752. *Proc. Natl. Acad. Sci. U.S.A.* **2006**, *103*, 2316–2321.

(12) Lutterbach, B.; Zeng, Q.; Davis, L. J.; Hatch, H.; Hang, G.; Kohl, N. E.; Gibbs, J. B.; Pan, B.-S. Lung Cancer Cell Lines Harboring MET Gene Amplification are Dependent on Met for Growth and Survival. *Cancer Res.* **2007**, *67*, 2081–2088.

(13) Engelman, J. A.; Zejnullahu, K.; Mitsudomi, T.; Song, Y.; Hyland, C.; Park, J. O.; Lindeman, N.; Gale, C. M.; Zhao, X.; Christensen, J.; Kosaka, T.; Holmes, A. J.; Rogers, A. M.; Cappuzzo, F.; Mok, T.; Lee, C.; Johnson, B. E.; Cantley, L. C.; Jänne, P. A. MET Amplification Leads to Gefitinib Resistance in Lung Cancer by Activating ERBB3 Signaling. *Science* **2007**, *316*, 1039–1043.

(14) Bean, J.; Brennan, C.; Shih, J.-Y.; Riely, G.; Viale, A.; Wang, L.; Chitale, D.; Motoi, N.; Szoke, J.; Broderick, S.; Balak, M.; Chang, W.-C.; Yu, C.-J.; Gazzdar, A.; Pass, H.; Rusch, V.; Gerald, W.; Huang, S.-F.; Yang, P.-C.; Miller, V.; Ladanyi, M.; Yang, C.-H.; Pao, W. MET Amplification Occurs With or Without T790M Mutations in EGFR Mutant Lung Tumors with Acquired Resistance to Gefitinib or Erlotinib. *Proc. Natl. Acad. Sci. U.S.A.* **2007**, *104*, 20932–20937.

(15) Zou, H. Y.; Li, Q. H.; Lee, J. H.; Arango, M. E.; McDonnell, S. R.; Yamazaki, S.; Koudriakova, T. B.; Alton, G.; Cui, J. J.; Kung, P.-P.; Nambu, M. D.; Los, G.; Bender, S. L.; Mroczkowski, B.; Christensen, J. G. An Orally Available Small-molecule Inhibitor of c-Met, PF-2341066, Exhibits Cytoreductive Antitumor Efficacy Through Antiproliferative and Antiangiogenic Mechanisms. *Cancer Res.* **2007**, *67*, 4408–4417.

(16) Bellon, S. F.; Kaplan-Lefko, P. J.; Yang, Y.; Zhang, Y.; Moriguchi, J.; Rex, K.; Johnson, C. W.; Rose, P. E.; Long, A. M.; O'Connor, A. B.; Gu, Y.; Coxon, A.; Kim, T.-S.; Tasker, A.; Burgess, T. L.; Dussault, I. c-Met inhibitors with Novel Binding Mode Show Activity against Several Hereditary Papillary Renal Cell Carcinoma-Related Mutations. *J. Biol. Chem.* **2008**, *283*, 2675–2683.

(17) Zhang, Y. H.; Kaplan-Lefko, P. J.; Rex, K.; Yang, Y.; Moriguchi, J.; Osgood, T.; Mattson, B.; Coxon, A.; Reese, M.; Kim, T.-S.; Lin, J.; Chen, A.; Burgess, T. L.; Dussault, I. Identification of a Novel Receptor d'Origine Nantais/c-Met Small-Molecule Kinase Inhibitor with Antitumor Activity in Vivo. *Cancer Res.* **2008**, *68*, 6680–6687.

(18) Raeppl, S.; Claridge, S.; Saavedra, O.; Gaudette, F.; Zhan, L.; Mannion, M.; Zhou, N.; Raeppl, F.; Granger, M.-C.; Isakovic, L.; Déziel, R.; Nguyen, H.; Beaulieu, N.; Beaulieu, C.; Dupont, I.; Robert, M.-F.; Lefebvre, S.; Dubay, M.; Rahil, J.; Wang, J.; Ste-Croix, H.; Macleod, A. R.; Besterman, J.; Vaisburg, A. N-(3-Fluoro-4-(2-arylthieno[3,2-b]pyridin-7-yloxy)phenyl)-2-oxo-3-phenylimidazolidine-1-carboxamides: A Novel Series of Dual c-Met/VEGFR2 Receptor Tyrosine Kinase Inhibitors. *Bioorg. Med. Chem. Lett.* **2009**, *19*, 1323–1328.

(19) Schroeder, G. M.; An, Y.; Cai, Z.-W.; Chen, X.-T.; Clark, C.; Cornelius, L. A. M.; Dai, J.; Gullo-Brown, J.; Gupta, A.; Henley, B.; Hunt, J. T.; Jeyaseelan, R.; Kamath, A.; Kim, K.; Lippy, J.; Lombardo, L. J.; Manne, V.; Oppenheimer, S.; Sack, J. S.; Schmidt, R. J.; Shen, G.; Stefanski, K.; Tokarski, J. S.; Trainor, G. L.; Wautlet, B. S.; Wei, D.; Williams, D. K.; Zhang, Y.; Zhang, Y.; Fagnoli, J.; Borzilleri, R. M. Discovery of N-(4-(2-Amino-3-chloropyridin-4-yloxy)-3-fluorophenyl)-4-ethoxy-1-(4-fluorophenyl)-2-oxo-1,2-dihydropyridine-

3-carboxamide (BMS-777607), a Selective and Orally Efficacious Inhibitor of the Met Kinase Superfamily. *J. Med. Chem.* **2009**, *52*, 1251–1254.

(20) Albrecht, B. K.; Harmange, J. C.; Bauer, D.; Berry, L.; Bode, C.; Boezio, A.; Chen, A.; Choquette, D.; Dussault, I.; Fridrich, C.; Hirai, S.; Hoffman, D.; Larrow, J. F.; Kaplan-Lefko, P.; Lin, J.; Lohman, J.; Long, A. M.; Moriguchi, J.; O'Connor, A.; Potashman, M. H.; Reese, M.; Rex, K.; Siegmund, A.; Shah, K.; Shimanovich, R.; Springer, S. K.; Teffera, Y.; Yang, Y.; Zhang, Y.; Bellon, S. F. Discovery and Optimization of Triazolopyridazines as Potent and Selective Inhibitors of the c-Met Kinase. *J. Med. Chem.* **2008**, *51*, 2879–2882.

(21) D'Angelo, N. D.; Bellon, S. F.; Booker, S. K.; Cheng, Y.; Coxon, A.; Dominguez, C.; Fellows, I.; Hoffman, D.; Hungate, R.; Kaplan-Lefko, P.; Lee, M. R.; Li, C.; Liu, L.; Rainbeau, E.; Reider, P. J.; Rex, K.; Siegmund, A.; Sun, Y.; Tasker, A. S.; Xi, N.; Xu, S.; Yang, Y.; Zhang, Y.; Burgess, T. L.; Dussault, I.; Kim, T.-S. Design, Synthesis, and Biological Evaluation of Potent c-Met Inhibitors. *J. Med. Chem.* **2008**, *51*, 5766–5779.

(22) Boezio, A. A.; Berry, L.; Albrecht, B. K.; Bauer, D.; Bellon, S. F.; Bode, C.; Chen, A.; Choquette, D.; Dussault, I.; Hirai, S.; Kaplan-Lefko, P.; Larrow, J. F.; Lin, M.-H. J.; Lohman, J.; Potashman, M. H.; Rex, K.; Santostefano, M.; Shah, K.; Shimanovich, R.; Springer, S. K.; Teffera, Y.; Yang, Y.; Zhang, Y.; Harmange, J.-C. Discovery and Optimization of Potent and Selective Triazolopyridazine Series of c-Met Inhibitors. *Bioorg. Med. Chem. Lett.* **2009**, *19*, 6307–6312.

(23) Nishii, H.; Chiba, T.; Morikami, K.; Fukami, T. A.; Sakamoto, H.; Ko, K.; Koyano, H. Discovery of 6-benzoyloxyquinolines as c-Met Selective Kinase Inhibitors. *Bioorg. Med. Chem. Lett.* **2010**, *20*, 1405–1409.

(24) Porter, J.; Lumb, S.; Lecomte, F.; Reuberson, J.; Foley, A.; Calmiano, M.; le Riche, K.; Edwards, H.; Delgado, J.; Franklin, R. J.; Gascon-Simorte, J. M.; Maloney, A.; Meier, C.; Batchelor, M. Discovery of a Novel series of Quinoxalines as Inhibitors of c-Met Kinase. *Bioorg. Med. Chem. Lett.* **2009**, *19*, 397–400.

(25) Porter, J.; Lumb, S.; Franklin, R. J.; Gascon-Simorte, J. M.; Calmiano, M.; Riche, K. L.; Lallemand, B.; Keyaerts, J.; Edwards, H.; Maloney, A.; Delgado, J.; King, L.; Foley, A.; Lecomte, F.; Reuberson, J.; Meier, C.; Batchelor, M. Discovery of 4-azaindoles as Novel Inhibitors of c-Met Kinase. *Bioorg. Med. Chem. Lett.* **2009**, *19*, 2780–2784.

(26) Buchanan, S. G.; Hendle, J.; Lee, P. S.; Smith, C. R.; Bounaud, P. Y.; Jessen, K. A.; Tang, C. M.; Huser, N. H.; Felce, J. D.; Froning, K. J.; Peterman, M. C.; Aubol, B. E.; Gessert, S. F.; Sauder, J. M.; Schwinn, K. D.; Russell, M.; Rooney, I. A.; Adams, J.; Leon, B. C.; Do, T. H.; Blaney, J. M.; Sprengeler, P. A.; Thompson, D. A.; Smyth, L.; Pelletier, L. A.; Atwell, S.; Holme, K.; Wasserman, S. R.; Emtage, S.; Burley, S. K.; Reich, S. H. SGX523 is an Exquisitely Selective, ATP-Competitive Inhibitor of the MET Receptor Tyrosine Kinase with Antitumor Activity in Vivo. *Mol. Cancer Ther.* **2009**, *8*, 3181–3190.

(27) Burgess, T.; Coxon, A.; Meyer, S.; Sun, J.; Rex, K.; Tsuruda, T.; Chen, Q.; Ho, S.-Y.; Li, L.; Kaufman, S.; McDorman, K.; Cattley, R. C.; Sun, J.; Elliott, G.; Zhang, K.; Feng, X.; Jia, X.-C.; Green, L.; Radinsky, R.; Kendall, R. Fully Human Monoclonal Antibodies to Hepatocyte Growth Factor with Therapeutic Potential Against Hepatocyte Growth Factor/c-Met-Dependent Human Tumors. *Cancer Res.* **2006**, *66*, 1721–1729.

(28) Martens, T.; Schmidt, N. O.; Eckerich, C.; Fillbrandt, R.; Merchant, M.; Schwall, R.; Westphal, M.; Lamszus, K. A Novel One-Armed Anti-c-Met Antibody Inhibits Glioblastoma Growth In Vivo. *Clin. Cancer Res.* **2006**, *12*, 6144–6152.

(29) Liu, X.; Yao, W.; Newton, R. C.; Scherle, P. A. Targeting the c-MET Signaling Pathway for Cancer Therapy. *Expert Opin. Invest. Drugs* **2008**, *17*, 997–1011.

(30) Migliore, C.; Giordano, S. Molecular Cancer Therapy: Can Our Expectation be MET? *Eur. J. Cancer* **2008**, *44*, 641–651.

(31) Pan, B.-S.; Chan, G. K. Y.; Chenard, M.; Chi, A.; Davis, L. J.; Deshmukh, S. V.; Gibbs, J. B.; Gil, S.; Hang, G.; Hatch, H.; Jewell, J. P.; Kariv, I.; Katz, J. D.; Kunii, K.; Lu, W.; Lutterbach, B. A.; Paweletz, C. P.; Qu, X.; Reilly, J. F.; Szewczak, A. A.; Zeng, Q.; Kohl, N. E.; Dinsmore, C. J. MK-2461, a Novel Multitargeted Kinase Inhibitor,

Preferentially Inhibits the Activated c-Met Receptor. *Cancer Res.* **2010**, *70*, 1524–1533.

(32) Wang, J.; Della Penna, K.; Wang, H.; Karczewski, J.; Connolly, T. M.; Koblan, K. S.; Bennett, P. B.; Salata, J. J. Functional and Pharmacological Properties of Canine ERG Potassium Channels. *Am. J. Physiol.: Heart Circ. Physiol.* **2003**, *284*, H256–H267.

(33) Dosed iv at 1 mg/kg as a solution in DMSO and po at 2 mg/kg as a solution in methylcellulose.

(34) To streamline the discussion, certain compounds prepared by specific standard one-off chemical transformations have not been fully described in these schemes. However the synthesis of each compound in this manuscript is completely described in the Experimental Section and the Supporting Information.

(35) Marcoux, J.-F.; Marcotte, F.-A.; Wu, J.; Dormer, P. G.; Davies, I. W.; Hughes, D.; Reider, P. J. A General Preparation of Pyridines and Pyridones via the Annulation of Ketones and Esters. *J. Org. Chem.* **2001**, *66*, 4194–4199.

(36) Brenner, D. G.; Halczenko, W.; Shepard, K. L. Imino-Bridged heterocycles II. Regiospecific Synthesis of the 1*H*-benzo[5,6]cyclohepta[1,2-*c*]pyridin-6,11-imine and 5*H*-benzo[4,5]cyclohepta[1,2-*b*]pyridin-5,10-imine Systems. *J. Heterocycl. Chem.* **1982**, *19*, 897–900.

(37) Wolfe, J. P.; Ahman, J.; Sadighi, J. P.; Singer, R. A.; Buchwald, S. L. An Ammonia Equivalent for the Palladium-Catalyzed Amination of Aryl Halides and Triflates. *Tetrahedron Lett.* **1997**, *38*, 6367–6370.

(38) Alcaraz, L.; Bennion, C.; Morris, J.; Meghani, P.; Thom, S. M. Novel *N*-Aryl and *N*-Heteroaryl Sulfamide Synthesis via Palladium Cross Coupling. *Org. Lett.* **2004**, *6*, 2705–2708.

(39) Winum, J.-Y.; Toupet, L.; Barragon, V.; Dewynter, G.; Montero, J.-L. *N*-(*tert*-Butoxycarbonyl)-*N*-[4-(dimethylazaniumylidene)-1,4-dihydropyridin-1-ylsulfonyl]azanide: A New Sulfamoylating Agent. Structure and Reactivity toward Amines. *Org. Lett.* **2001**, *3*, 2241–2243.

(40) Yang, B. H.; Buchwald, S. L. Palladium-Catalyzed Amination of Aryl Halides and Sulfonates. *J. Organomet. Chem.* **1999**, *576*, 125–146.

(41) Hartwig, J. F. Transition Metal Catalyzed Synthesis of Arylamines and Aryl Ethers from Aryl Halides and Triflates: Scope and Mechanism. *Angew. Chem., Int. Ed.* **1998**, *37*, 2046–2067.

(42) Wolfe, J.; Wagaw, S.; Marcoux, J.-F.; Buchwald, S. L. Rational Development of Practical Catalysts for Aromatic Carbon–Nitrogen Bond Formation. *Acc. Chem. Res.* **1998**, *31*, 805–818.

(43) Netherton, M. R.; Fu, G. C. Air-Stable Trialkylphosphonium Salts: Simple, Practical, and Versatile Replacements for Air-Sensitive Trialkylphosphines. Applications in Stoichiometric and Catalytic Processes. *Org. Lett.* **2001**, *3*, 4295–4298.

(44) c-Met IC₅₀ refers to the ability to inhibit the phosphorylation of a synthetic peptide by the cytosolic portion of recombinant human c-Met, as measured in an HTRF assay. See Experimental Section details and ref 31 for a complete description.

(45) Giordano, S.; Ponzetto, C.; Di Renzo, M. F.; Cooper, C. S.; Comoglio, P. M. Tyrosine Kinase Receptor Indistinguishable from the c-Met Protein. *Nature* **1989**, *339*, 155–156.

(46) Measured at Essen Biosciences in Chinese hamster lung cells (<http://essenbioscience.com/services/CardiacSafety.html>).

(47) Methanesulfonamide **47** has a calculated (ACD laboratories) p*K*_a = 8.87 ± 0.20, while **57** has a calculated p*K*_a = 4.23 ± 0.20.

(48) Identified by incubating the compound with rat and human hepatocytes and analysis of metabolites via HPLC and mass spectrometry.

(49) Monomethyl **71** has been identified as a major metabolite of **59** in rat hepatocytes.

(50) Rickert, K. W.; Patel, S. B.; Allison, T. J.; Byrne, N. J.; Darke, P. L.; Ford, R. D.; Guerin, D. J.; Hall, D. L.; Kornienko, M.; Lu, J.; Munshi, S. K.; Reid, J. C.; Shipman, J. M.; Stanton, E. F.; Wilson, K. J.; Young, J. R.; Soisson, S. M.; Lumb, K. J. Structural Basis for Selective Small-Molecule Inhibition of the Phosphorylated c-Met Kinase Domain. *J. Biol. Chem.* **2011**, *286*, 11218–11225.

(51) As predicted by density-functional theory (DFT) geometry calculations at the B3LYP/6-31 g* level.

(52) Berthou, S.; Aebersold, D. M.; Schmidt, L. S.; Stroka, D.; Heigl, C.; Streit, B.; Stalder, D.; Gruber, G.; Liang, C.; Howlett, A. R.; Candinas,

D.; Greiner, R. H.; Lipson, K. E.; Zimmer, Y. The Met Kinase Inhibitor SU11274 Exhibits a Selective Inhibition Pattern Toward Different Receptor Mutated Variants. *Oncogene* **2004**, *23*, 5387–5393.

(53) Qi, J.; McTigue, M. A.; Rogers, A.; Lifshits, E.; Christensen, J. G.; Jänne, P. A.; Engelman, J. A. Multiple Mutations and Bypass Mechanisms Can Contribute to Development of Acquired Resistance to MET Inhibitors. *Cancer Res.* **2011**, *71*, 1081–1091.

(54) Dussault, I.; Bellon, S. F. c-Met Inhibitors with Different Binding Modes. *Cell Cycle* **2008**, *7*, 1157–1160.

(55) For an enantioselective synthesis of **81**: Stewart, G. W.; Brands, K. M. J.; Brewer, S. E.; Cowden, C. J.; Davies, A. J.; Edwards, J. S.; Gibson, A. W.; Hamilton, S. E.; Katz, J. D.; Keen, S. P.; Mullens, P. R.; Scott, J. P.; Wallace, D. J.; Wise, C. S. Process Development and Large-Scale Synthesis of a c-Met Kinase Inhibitor. *Org. Process Res. Dev.* **2010**, *14*, 849–858.